Reappraisal of the 1887 Ligurian earthquake (western Mediterranean) from macroseismicity, active tectonics and tsunami modelling

C. Larroque, Oona Scotti, M. Ioualalen

Geophysical Journal International

Geophys. J. Int. (2012) **190,** 87–104 doi: 10.1111/j.1365-246X.2012.05498.x

Reappraisal of the 1887 Ligurian earthquake (western Mediterranean) from macroseismicity, active tectonics and tsunami modelling

Christophe Larroque,[1] Oona Scotti[2] and Mansour Ioualalen[3]

[1] *Géoazur, UMR* 7329 *CNRS,* 250 *rue A. Einstein, Valbonne* 06560*, France. E-mail: larroque@geoazur.unice.fr*
[2] *DEI/SARG/BERSSIN, Institut de radioprotection et sureté nucléaire, B.P.*17*, Fontenay-aux-Roses Cedex,* 92262*, France*
[3] *Géoazur, UMR* 7329 *IRD-CNRS-UPMC-UNSA,* 2 *quai de la Darse, Villefranche-sur-mer,* 06230*, France*

Accepted 2012 April 4. Received 2012 April 4; in original form 2011 December 13

SUMMARY

Early in the morning of 1887 February 23, a damaging earthquake hit the towns along the Italian and French Riviera. The earthquake was followed by a tsunami with a maximum run-up of 2 m near Imperia, Italy. At least 600 people died, mainly due to collapsing buildings. This 'Ligurian earthquake' occurred at the junction between the southern French–Italian Alps and the Ligurian Basin. For such a historical event, the epicentre and the equivalent magnitude are difficult to characterize with any degree of precision, and the tectonic fault responsible for the earthquake is still under debate today. The recent MALISAR marine geophysical survey allowed the identification of a large system of active faults. We propose that the rupture of some of the segments belonging to this 80-km-long northern Ligurian Faults system connected to a shallow-dipping major thrust plane at depth was the source of the 1887 Ligurian earthquake. We investigated the macroseismic data from the SISFRANCE-08 and DBMI-04 historical databases using several models of intensity attenuation with distance and focal depth. The modelling results are consistent with the off-shore location, with an epicentre around 43.70°–43.78°N and 7.81°–8.07°E, and with a magnitude M_w in the range of 6.3–7.5. Numerous earthquake source scenarios have been tested on the tide gauge record at Genoa harbour. As a result, we present seven characteristic source earthquake scenarios for a shallow strong earthquake occurring below the northern Ligurian margin. The modelled tide gauge records were analysed with the help of basic statistical tools and a simple harmonic analysis, to extract the wave spectrum characteristics. This analysis indicates that scenarios of a magnitude M_w of 6.8–6.9 along a reverse N55°E striking fault are the best candidates to explain the known characteristics of the tsunami that followed. The best-fitting scenarios comprise a 70°-dipping southward fault plane with M_w 6.8 and a 16°-dipping northward fault plane with M_w 6.9, both with reverse kinematics. Taking into account the geometry of the active faults, the location of the macroseismic epicentre and the morphotectonic evolution of the continental slope, we propose that the 1887 Ligurian earthquake corresponded to the reverse faulting of a N55°E striking fault plane dipping to the north with a coseismic slip of 1.5 m.

Key words: Tsunamis; Palaeoseismology; Seismicity and tectonics; Continental neotectonics; Dynamics: seismotectonics; Europe.

INTRODUCTION

Strong historical earthquakes are of importance as they provide relevant information on the associated deformation zone and seismic hazard. This is all the more true in areas of low deformation rate, where strong earthquakes are particularly infrequent (e.g. Camelbeeck *et al.* 2001; Bakun & Hopper 2004). Seismic hazard assessment involves a preliminary step that leads to the characterization of earthquake potential (location, maximum magnitude, kinematics, and recurrence period; Reiter 1990). In populated areas, historical earthquakes are often documented, and in cases of an optimal distribution of the macroseismic data, this allows the seismic source to be defined (e.g. Levret *et al.* 1994; Gasperini *et al.* 1999; Bakun & Scotti 2006), although the active fault responsible for the earthquake is often difficult to identify (e.g. Meyer *et al.* 1994; Ferry *et al.* 2005).

The Alps-Ligurian Basin junction (Fig. 1) is a low deformation rate area that suffered several historical earthquakes: for the

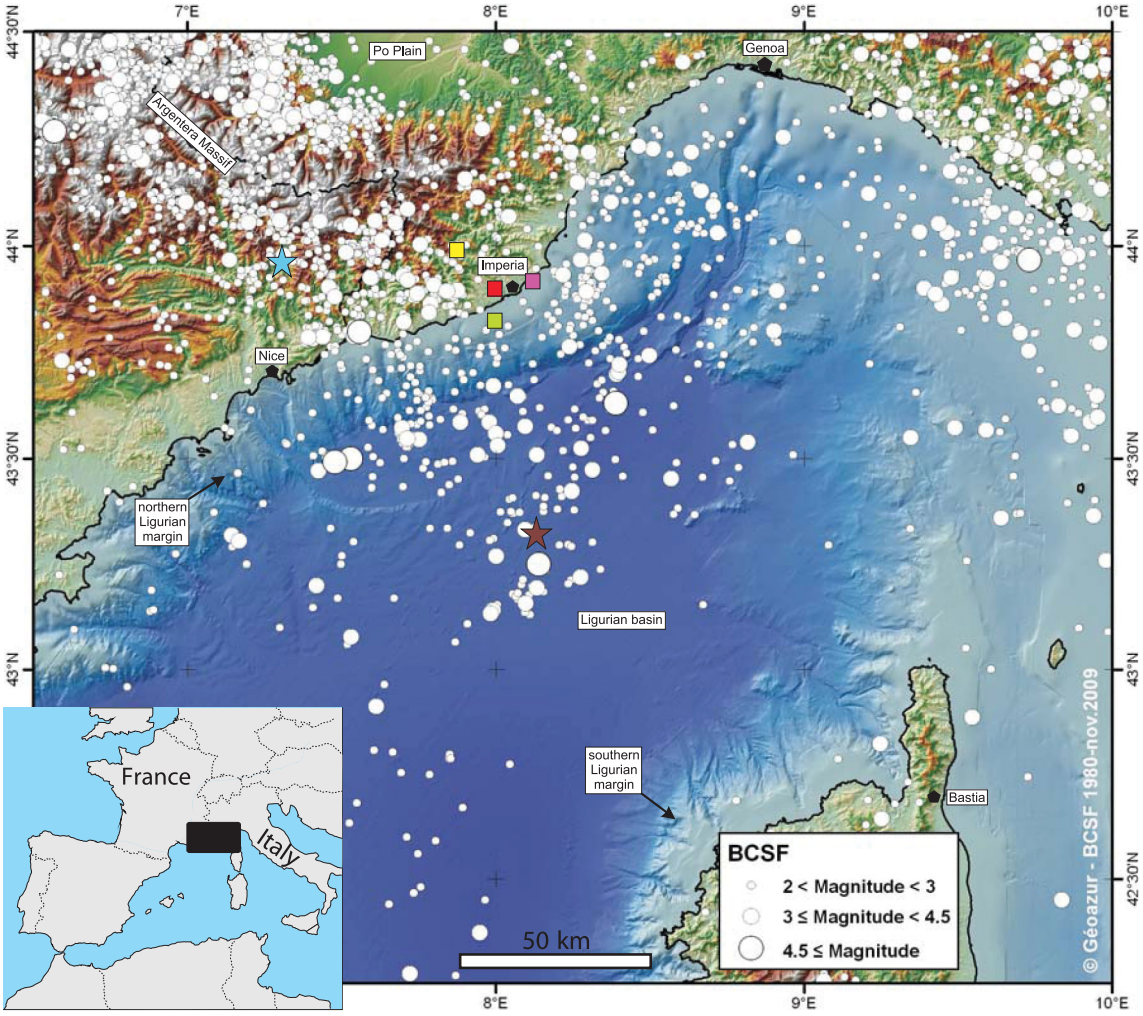

Figure 1. Seismicity map of the Alps–Ligurian Basin junction recorded from 1980 to 2010 January (catalogue from the Bureau Central Sismologique Français, http://www.franceseisme.fr/). The DTM is a compilation of various data from the French Institut Géographique National (IGN), the Shuttle Radar Topography Mission (SRTM, NASA) and marine surveys of the Institut Français de Recherche et d'Exploration de la Mer (IFREMER). The magnitude range is from 2 to 4.7. The coloured stars correspond to the approximate epicentres of the 1564 July 20, earthquake (blue; I, VIII MCS) and the 1963 July 19, earthquake (brown, M_L 6.0). The coloured squares correspond to the previous locations of the 1887 February 23, earthquake (I, IX MSK); from CFTI4-med (red), SISFRANCE (green), and two locations from the boxer model (yellow and purple; P. Gasperini, personal communication, 2011).

period of 1182 A.D. to 1965, more than 130 events with intensities greater than V on the Medvedev–Sponheuer–Karnik (MSK) or Mercali–Cancani–Sieberg (MCS) scales are registered in the macroseismic catalogues (DBMI 2004, hereafter DBMI-04; SISFRANCE 2008, hereafter SISFRANCE-08; Larroque 2009). At a regional scale, these active faults are poorly characterized and their properties remain widely unknown (e.g. Courboulex *et al.* 2007; Larroque *et al.* 2011a). However, strong historical earthquakes can be major reference points to indicate what type of event might be possible in any region. The need to improve the regional seismic hazard of zones of low deformation rate and high vulnerability is thus a scientific challenge that has a high social demand; therefore, we must focus on these details to make the most of the available historical events.

The 1887 Ligurian earthquake was the strongest event recorded in the southwestern Alps-Liguria area over the last 1000 yr, and as such, it has become an emblematic event. Its location (on-shore versus off-shore) and magnitude (current estimates from 5.6 to 6.5) have been discussed for many years (e.g. Capponi *et al.* 1985; Tinti *et al.* 1987; Ferrari 1991; Boschi *et al.* 1995; Guidoboni *et al.* 2007), and the fault that produced it remains to be defined. Following this earthquake, there were different phenomena that were described in various manuscripts, including electrical effects (Poirier *et al.* 2008), and in particular, a tsunami along the Ligurian coast (e.g. Denza 1887).

The Ligurian Sea is one of the 'tsunamigenic' zones of the northern Mediterranean (Soloviev 1990; Tinti *et al.* 2004). Two of the tsunamis that have occurred there are suspected to have been earthquake induced: the 1887 event, and potentially the 1564 event (Fig. 1). Some other tsunamis have been related to submarine slope failures, such as the 1979 Nice event. Although the macroseismic databases contain inconsistencies and hydrographic data are few, these remain the best available data sets, and their joint study along with the active tectonic data allows a reasonable analysis of the 1887 event. Following the previous study of Eva & Rabinovich (1997), we reappraise the 1887 event, taking into account, on the one hand, the French and Italian macroseismic databases (SISFRANCE-08 and DBMI-04) and the recent intensity attenuation models of

Bakun & Scotti (2006), and on the other hand, the new structural and bathymetric data obtained during the MALISAR geophysical survey (Larroque *et al.* 2011b). The objective of this study was thus twofold: (1) to estimate the location and magnitude of the 1887 Ligurian earthquake, to provide reasonable seismic scenarios and (2) to determine which seismic scenario better fits the data, by modelling the tsunami that was associated with this earthquake (Larroque *et al.* 2010).

SEISMOTECTONIC CONTEXT AND GEOLOGICAL EVOLUTION

The Alps–Ligurian Basin junction is one of the most seismically active areas in western Europe. It is at present characterized by continuous low-to-moderate seismic activity (Béthoux 1992; Baroux *et al.* 2001; Larroque *et al.* 2001). This seismicity affects a wide area both on-shore and off-shore (Fig. 1). The focal depths of the earthquakes are generally shallow, at between 5 and 20 km in depth. The distribution of the seismicity is mainly diffuse, except in some cases that have allowed the imaging of active fault planes (e.g. Courboulex *et al.* 2007; Turino *et al.* 2009). Three strong historical earthquakes have successively affected this area (Fig. 1): the so-called 'Nissart' earthquake in 1564 (I, VIII MCS), which was probably located some tens of kilometres north of Nice (Vogt 1992), the so-called 'Ligurian' earthquake in 1887 (I, IX MSK), which was close to the coast, and the 1963 July 19, event (M_L 6.0; Bossolasco *et al.* 1972), farther south in the basin.

Over the past 100 Myr, the kinematic evolution of the western European margin has been dominated by the convergence between the Africa and Eurasia plates, which led to subduction of the Tethyan Ocean, and then to the collision between these continental blocks (Dercourt *et al.* 1986; Dewey *et al.* 1989). During this long convergence period, the Ligurian Basin opened. The continental rifting started between 34 and 28 Myr and ended at around 21 Myr. This was followed by a drifting phase, between 21 and 16 Myr, that was associated with most of the counterclockwise rotation of the continental Corsica-Sardinia block (Westphal *et al.* 1976; Réhault *et al.* 1984; Séranne 1999; Edel *et al.* 2001; Speranza *et al.* 2002; Gattacceca *et al.* 2007). The Ligurian Basin is considered to be a backarc basin that was generated from the southeastward roll-back of the Apennines–Maghrebides subduction zone (Le Pichon 1982; Malinverno & Ryan 1986; Doglioni *et al.* 1997; Faccenna *et al.* 1997). As a consequence of this past geological history, the southwestern Alps–Ligurian Basin junction is a particularly complex topographic and structural domain that has a strong tectonic and topographic inheritance and large cumulated deformation.

Recent GPS measurements attest to a very low strain rate in the southwestern Alps–Ligurian Basin area (Larroque *et al.* 2009). The convergence of the Africa (Nubia) Plate towards Eurasia now occurs at a rate of 4–5 mm yr^{-1} in a N309° ±5° direction at the longitude of the western Alps (Nocquet & Calais 2003; McClusky *et al.* 2003; Nocquet *et al.* 2006), with the shortening mainly occurring along the Maghrebides (Nocquet & Calais 2004; Serpelloni *et al.* 2007). Therefore, the major part of the current deformation north of the Maghrebides is most probably not related to Nubia/Eurasia motion and, the Alps–Ligurian Basin junction is now an intraplate region (Larroque 2009). From a geodynamic point of view, the question remains why strong earthquakes can occur in such a region when it has now been shown that the present-day Eurasia–Nubia Plate boundary is located further south.

STRUCTURES OF THE NORTHERN LIGURIAN MARGIN

On-shore geophysical surveys and modelling have shown that the Moho is at a 45–50 km depth under the high topography (up to 3200 m) of the Argentera Massif, and that it becomes shallower towards the south, to reach a depth of around 20–25 km under the coast (Masson *et al.* 1999; Béthoux *et al.* 2007; Thouvenot *et al.* 2007; Schreiber *et al.* 2010; Dessa *et al.* 2011). Off-shore, the continental crust thins at a few tens of kilometres from the coast, and in the basin the atypical oceanic crust is 4 km thick (Chamot-Rooke *et al.* 1999).

The structure of the Ligurian Sea consists of (Fig. 1): (1) a northern extensional margin with ENE-trending grabens that are mainly bound by SE-dipping normal faults; (2) a central and relatively flat oceanic part and (3) the southeastern margin of Corsica-Sardinia, the internal structures of which remain poorly known (Réhault *et al.* 1984; Contrucci *et al.* 2001; Rollet *et al.* 2002). The major known structures of the Ligurian Sea result from the Neogene rifting and spreading. However, currently along the northern Ligurian margin, the state of stress corresponds to a compressive tectonic regime (e.g. Béthoux *et al.* 1992). This compressive state of stress appears to be a paradox along a passive margin, although it is a common situation in the western Mediterranean setting. For instance, the Algerian margin shows the same features (e.g. Rebaï *et al.* 1992; Déverchère *et al.* 2005), and this situation can be found along several passive margins around the world (Cobbold 2008). Some previous studies have attempted to identify geological evidence of compressive deformation on the margin, but the available data were not sufficiently accurate (Chaumillon *et al.* 1994; Larroque *et al.* 2001; Bigot-Cormier *et al.* 2004).

The recent MALISAR geophysical survey was dedicated to the characterization of the active tectonics and submarine landslides from Nice to Genoa, with the collection of a comprehensive set of detailed geophysical data, which included mainly high-resolution multibeam bathymetry, multichannel seismic reflection profiles, and backscattered imagery (Mercier de Lépinay *et al.* 2007; Migeon *et al.* 2009). Following a detailed morphotectonic analysis, a set of N60–70°E scarps at the foot of the northern Ligurian margin was identified (Fig. 2a). These scarps result from the cumulated offsets along faults during Plio-Quaternary times: the kinematics of faulting is mainly reverse, with a small strike-slip component that has not be precisely defined. Several segments of variable lengths have been revealed between 43°30′N–7°30′E and 44°N–8°45′E (Larroque *et al.* 2011b). These faults dip to the north and cut across the northern part of the basin and the continental slope.

The most prominent feature of the margin is the Imperia Promontory (northeastern margin, Fig. 2a): a 40-km-long ridge with an elevation of around 1600 m above the basin floor. The base of the promontory is bound by three N60°E active faults that we call the Ligurian Faults system (LFS). On the northwestern margin, the so-called 'Marcel Fault' shows evidence of present-day activity (Fig. 2b): the location and the focal mechanisms of the four moderate earthquakes that took place around this 10-km-long fault plane have allowed us to ascribe the 1989 and the 2001 events to the Marcel Fault ($M_L = 4.5$ and 4.6, respectively).

From the focal mechanisms and from the geometry of the active LFS it now appears difficult to accept the interpretation of Fanucci & Nicolich (1984), who suggested that normal faulting dominates the active deformation of the northern Ligurian margin; or the proposal of Eva & Rabinovich (1997), who suggested that the activation of one of the normal faults arising from the rifting accounted for the

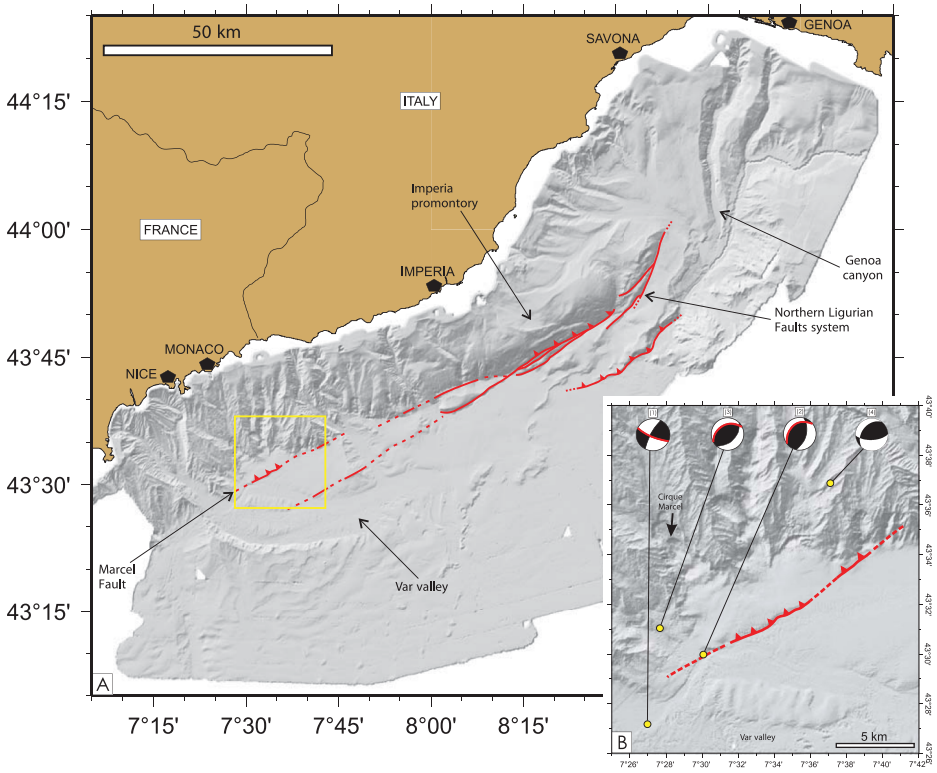

Figure 2. (A) Structural sketch of the northern Ligurian Faults system (modified from Larroque *et al.* 2010a). At the foot of the northern Ligurian margin, there are several faults oblique to the margin direction, which are 80 km long, extending from Nice (7°15'E) to Savona (8°30'E). The yellow rectangle corresponds to the inset (B). (B) Focal mechanisms of the moderate earthquakes associated with the Marcel Fault. (1) 1986 May 1, $M_L = 3.8$; (2) 1989 December 26, $M_L = 4.5$; (3) 2001 February 25, $M_L = 4.6$; (4) 2009 April 21, $M_L = 3.0$. The epicentres are located with an error in the range of 5 and 2 km for the events of 1986–1989 and 2001–2009, respectively. Red on the DTM, trace of the fault. The probable fault planes are in red on the focal mechanisms.

Table 1. Characteristics of the seismic sequence of the 1887 February 22–23, from the CFTI4MED database (http://storing.ingv.it/cfti4med/) and from the SISFRANCE database (http://www.sisfrance.net/). The different timings between the databases are due to the different time scales employed in France and Italy at the time of the earthquake.

	CFTI4MED			SISFRANCE			
Date	Hour	MCS	Location	Hour	MSK	Location	Type
1887 February 22	–	–	–	21:00	N/A		Foreshock
1887 February 23	05:22	IX	43.883°N 8.00°E	05:50	IX	43.83°N 8.00°E	Main shock
1887 February 23	05:29	N/A	–	06:10	N/A	–	Aftershock
1887 February 23	07:51	N/A	–	08:30	VII	43.833°N-8.00°E	Aftershock

1887 Ligurian earthquake (see also discussion in Augliera *et al.* 1994); and we also disagree with the location and geometry of the composite seismogenic source proposed by Basili *et al.* (2008) who suggested that the 1887 earthquake occurred on an E–W reverse fault near Imperia. However, the detailed geophysical data from the MALISAR surveys does not allow us to precisely identify the fault that slipped during the 1887 event.

THE 1887 LIGURIAN EARTHQUAKE: RELOCATION AND MAGNITUDE

The main shock of the Ligurian earthquake of the 1887 February 23, was felt across a vast area that covered Switzerland and Austria to the north, and that reached as far as the eastern Pyrenees to the west and northern Sardinia to the south (SISFRANCE-08 and DBMI-04). In the following year, approximately 200 aftershocks were identified. Major damage occurred along the 100 km coastline between Menton (France) and Albissola (Italy), and between the coast and 20 km inland, in the mountainous regions of the southwestern Alps and northern Apennines that rise immediately from the coast (e.g. Fines 1887; Meunier 1887; Offret 1887; Stephan 1887; Taramelli & Mercalli 1888; Capponi *et al.* 1985; Ferrari 1991). Almost 300 villages were affected by damage, 200 of which suffered great destruction. It is important to note that all of the localities that suffered the most from the main-shock were again affected by two strong aftershocks that occurred the same morning (Table 1).

Data

Two sets of macroseismic intensity assignments are available for the 1887 event: one in the SISFRANCE-08 database, and one in the DBMI-04 database. The geographical areas covered by the two data sets differ (Fig. 3), as the French data set covers France and parts of Italy, and the Italian data set is definitely more complete in Italy.

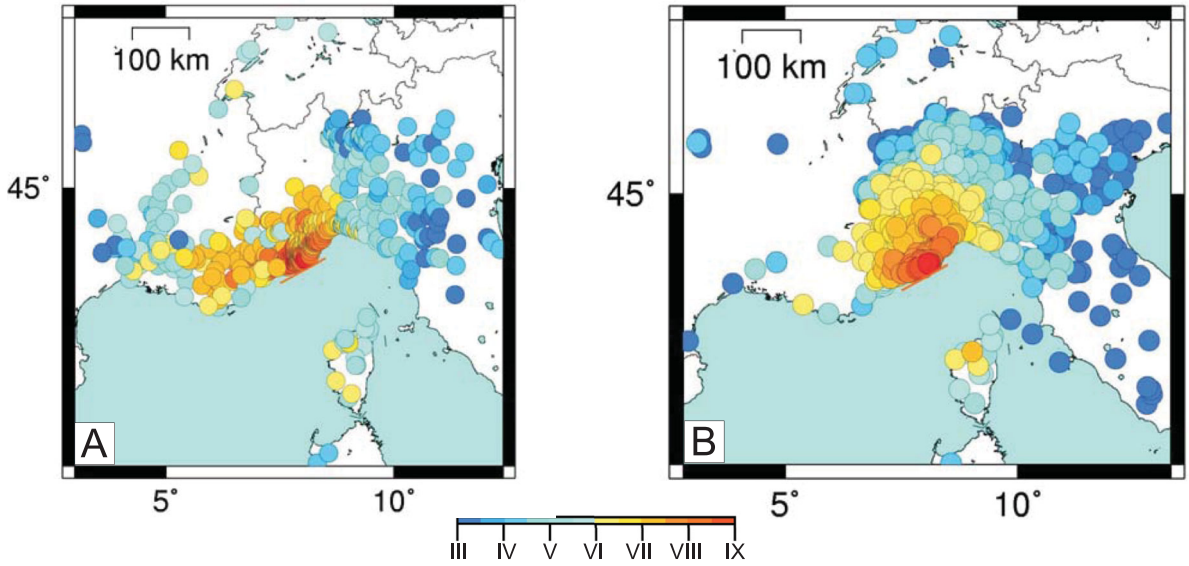

Figure 3. Geographical distribution of the intensity data points that are available for the 1887 Ligurian earthquake: (A) the SISFRANCE (2008 version) and (B) the DMBI (2004 version) macroseismic databases.

It is beyond the scope of this study to combine and merge these two data sets: they are used here as they are provided by the databases, to obtain a range of possible values for the location and magnitude of the 1887 earthquake.

The two data sets provide two different interpretations of the available documentation concerning this earthquake. The interpretations differ not only in terms of the spatial distributions and the intensity evaluations for the same locations, but also in terms of the timing of the sequence (see Table 1). Universal time zones were not yet widely established in the world at the time of this earthquake, and in particular, French and Italian times differed by 20–30 min, depending on whether the mean Paris, mean Rome, or local train station times are referenced in the documents. A dedicated study that merges the entire documentary sources for this sequence of events and that provides a homogeneous evaluation of the intensity data would help to address the inconsistencies between these two data sets. In this study, we preferred to keep each data set separate, such that we can address the issues from the point of view of having two 'views' of the same event, through the analysis of different sources, with different methodologies, and at different intensity scales.

Assumptions and uncertainties

The intensity assignments of the 1887 event are affected by numerous uncertainties. The most important one concerns the known cumulative effects for the localities that suffered the main shock and the two strong aftershocks. The second source of uncertainty isthat many of the sites in the source region are located along the coast and were potentially affected by local site effects, which might have amplified their intensity assignments. This implies that magnitude estimates in our study may represent upper boundary values. A third source of uncertainty comes from these two independent data sets themselves. Not only do the two data sets contain quite different isoseismal fields, but they also provide intensity assignments based on different intensity scales (MSK for SISFRANCE, and MCS for DBMI). Following the suggestions of Musson *et al.* (2010), this study assumes that these two scales are equivalent over the entire range. Implementation of a MCS to MSK conversion factor, as suggested by Levret & Mohammadioun (1984), would lead to lower intensity values for intensities greater than VI MCS and thus to lower magnitude estimates for the DBMI-04 data set.

Finally, magnitude and location estimates are affected by uncertainties that are intrinsic to the methodology used. In this study, we used the same method as that used by Bakun & Scotti (2006), who combined the Bakun & Wentworth (1997) technique with bootstrap resampling (Efron 1982). This approach provides objective, reproducible estimates of location uncertainties and can be applied to all historical earthquakes with more than a few intensity assignments. Because the location uncertainty in the Bakun & Scotti (2006) intensity prediction models also depends on depth, two depths, 10 and 20 km, were tested, covering the range of instrumental depths estimated in the source region of the 1887 event (Bossolasco *et al.* 1972; Déverchère *et al.* 1991; Augliera *et al.* 1994; Eva *et al.* 2001; Béthoux *et al.* 2008).

Choice of an intensity prediction model

The estimation of the magnitude and depth of historical earthquakes requires the appropriate choice of an intensity prediction equation, which is sometimes referred to as an intensity attenuation model. The Provence intensity attenuation model proposed by Bakun & Scotti (2006) is well suited to this study, as it is based on data from a geographical region that coincides to a large extent with that of the 1887 earthquake. The coefficients of the Provence intensity prediction equation are the following:

$$\mathrm{MSK} = 3.98 + 1.27M - 3.41 \times \log \Delta h,$$

where M is the macroseismic moment magnitude and Δh is the hypocentral distance (in km).

Results

The location and magnitude estimates for the 1887 event based on the Provence intensity model are shown in Fig. 4. The difference in

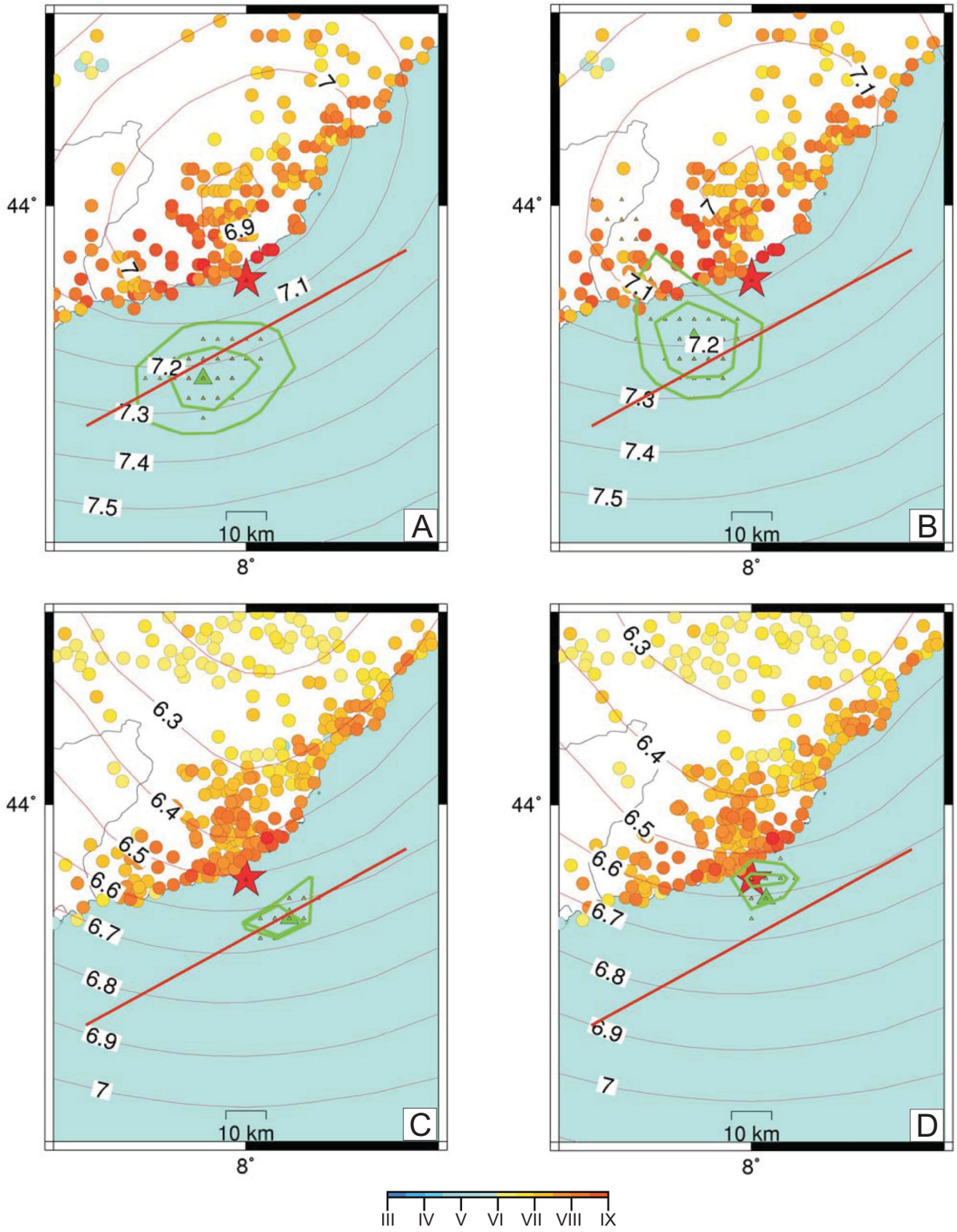

Figure 4. Location and magnitude estimates for the 1887 event based on the SISFRANCE-08 data set (hypocentre at 10 km depth in A, and 20 km depth in B) and the DBMI-04 database (hypocentre at 10 km depth in C, and 20 km depth in D). Red contours represent the intensity magnitude (M_i) estimate of the event at each trial location, assuming the Provence intensity model of Bakun & Scotti (2006). The intensity centre (IC) represents the trial source location for which the root mean square of M_i values is minimum (see Bakun & Scotti 2006, for more details on the methodology). The green triangles represent the bootstrap IC, and the green contours represent the corresponding 67 and 95 per cent confidence limits for the location (100 bootstrap runs). The red star represents the location provided in the SISFRANCE-08 database. The NE-SW brown line represents the location of the potential source region of the 1887 event as deduced, from Fig. 2.

Table 2. Epicentre locations and moment magnitudes determined in this study from the SISFRANCE and the DBMI databases for the 1887 February 23, earthquake.

Database	Latitude (°N)	Longitude (°S)	M_w
SISFRANCE-08	43.65	7.82	6.8–7.5
DBMI-04	43.78	8.07	6.3–6.9

the spatial distribution and intensity assignments between the two macroseismic data sets results in two quite different estimates of magnitude and location for this event. The magnitude estimates are higher for the SISFRANCE-08 data set, compared to the DBMI-04 data set. The 67 and 95 confidence contours for the location are wider for the SISFRANCE-08 data set, compared to the DBMI-04 data set, indicative of a data set that has a greater resolving power in the source region. Indeed, the dense distribution of high intensity assignments i6n the DBMI-04 region constrains the location to within ±5 km. The influence of the depth is more evident for the DBMI-04 data set, where the 10-km-deep hypothesis forces the intensity centre further out to sea compared to the 20-km-deep hypothesis (Fig. 4d).

Taking into account the uncertainties at the 2σ level, the epicentral location of the 1887 earthquake is estimated to have been at sea (Table 2), most likely between 43.65°N and 7.82°E from the SISFRANCE-08 database, and 43.78°N–8.07°E for the DBMI-04 database. The magnitude is estimated at the 1σ level as between $6.8 < M_w$SISFRANCE-08 < 7.5 and between $6.3 < M_w$DBMI-04 < 6.9. If the Alps intensity attenuation model of Bakun & Scotti (2006) were applied instead, the magnitude estimates would be higher for both the Italian and French data sets.

It is worth noting that differences in the distributions of the macroseismic points between the two data sets do not result in major differences in the estimated locations of the earthquake. This implies that statistically speaking, the relative distributions of macroseismic intensity values in the epicentral region are equivalent between the two data sets. The most important difference remains the absolute intensity evaluation, which is on average higher for the SISFRANCE-08 database, compared to the DBMI-04 database.

To reduce the uncertainties that affect the macroseismic data sets of the 1887 event, an estimate of the best magnitude and location values based exclusively on intensity assignments would require the re-evaluation of the intensity estimates for the two data sets combined, which is beyond the scope of this study. For the purpose of this study, it suffices to say that the DBMI-04 data set appears to be the one that best constrains the location of the 1887 event, due to a more dense distribution of high intensity values. On this basis, the best location for this earthquake is most likely between the coast close to the SISFRANCE epicentre and the LFS identified by the MALISAR survey (Figs 2 and 4), which is consistent with the north dipping LFS structure. The analysis of the tsunami recording in the following paragraphs will help to further reduce the range of possible magnitudes and depth estimates by identifying the scenarios that best fit the tide gauge observation.

THE EARTHQUAKE-INDUCED TSUNAMI

Following the main shock, sudden movements of the sea surface were observed from Marseille (France) to Livorno (Italy) (Fig. 5).

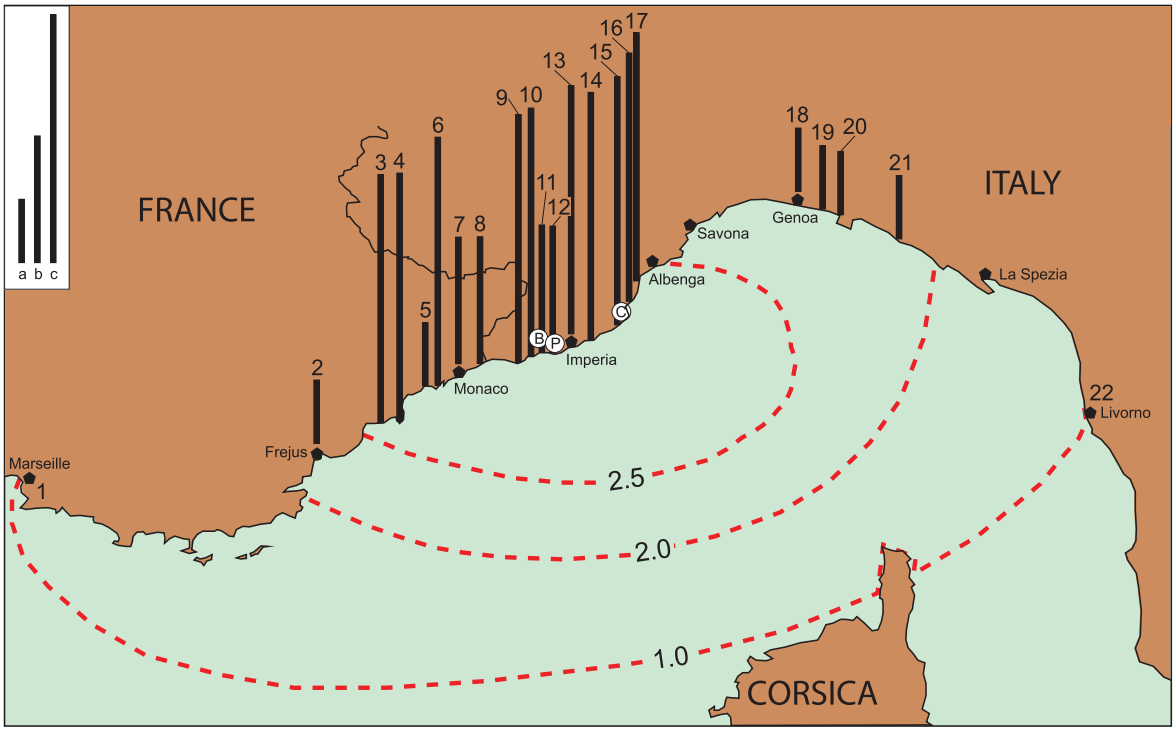

Figure 5. Consequences of the 1887 February 23, earthquake observed along the coast from Marseille (France) to Livorno (Italy). The red dotted lines correspond to the distribution of the intensity of the tsunami [intensity scale from Sieberg (1923) modified by Ambraseys (1962), compilation by A. Laurenti]. The black bars are local run-up observations : $0 < a < 0.5$ m; $0.5 < b < 1$ m; $1 < c < 2$ m. Locations: 1, Marseille; 2, Fréjus; 3, Cannes; 4, Antibes; 5, Nice; 6, St Jean-Cap-Ferrat; 7, Monaco; 8, Menton; 9, Ospedaletti; 10, San Remo; 11, Arma di Taggia; 12, Riva Ligure; 13, Imperia; 14, Oneglia; 15, Diano Marina; 16, Andora; 17, Alassio; 18, Genoa; 19, Bogliasco; 20, Recco; 21, Sestri Levante; 22, Livorno. B, Bussana; P, Pompeiana; C, Cervo and San Bartolomeo del Cervo.

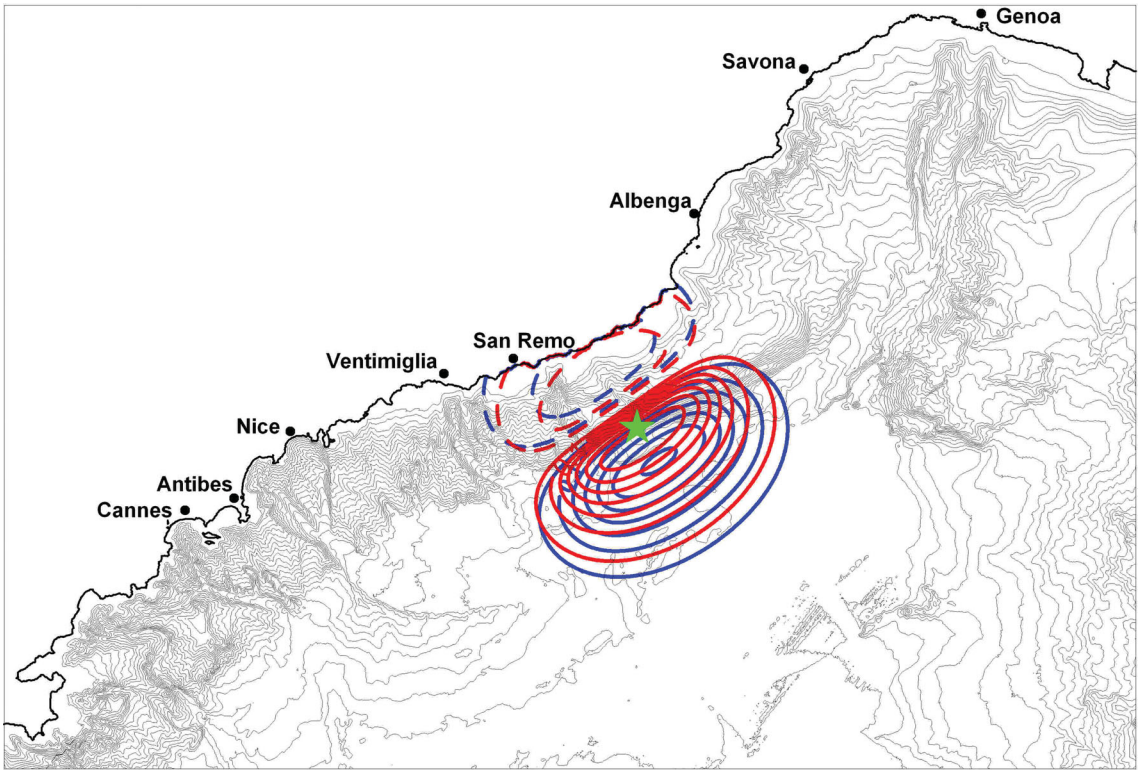

Figure 6. The computational domain (43°05'N–44°27'N; 6°32'E–9°15'E), including the bathymetric field (100 m isolevels) and the associated initial tsunami at its generation; that is, the seafloor coseismic deformation (dashed lines are for subsidence and full lines are for uplift, with 5 cm iso-contours) for scenario S6 (blue) and S7 (red) of Table 3. The green star corresponds to the earthquake epicentre.

The tsunami was not destructive, and over 500 km the main observations correspond to small oscillations along the coast near Marseille and sea-surface elevations with maximum run-up in the range of 1–2 m from Antibes to Albenga. The main observations were along the Ligurian coast near Imperia (Fig. 5). The tsunami was not recorded over the rest of the western Mediterranean, and no run-up was noted in Corsica, a situation certainly related to the epicentre being located close to the northern Ligurian margin. The tide gauge of Marseille did not record any significant signal, while the tide gauges of the Nice and Genoa harbours recorded the sea-surface oscillations precisely. Some very small oscillations were mentioned by people who observed the sea surface near Marseille and Livorno (Denza 1887; Lallemand 1887; Naudin 1887; Bianchi 1888; Taramelli & Mercalli 1888; Eva & Rabinovich 1997; Pelinovsky *et al.* 2002).

To model the tsunami, we took into account the new structural and bathymetric data that are available for the northern Ligurian margin (see below) and our results on the macroseismic hypocentre location and magnitude. We propose that the faulting of part of the 80-km-long LFS (Fig. 2a) was the source of the 1887 Ligurian earthquake. The preferred hypocentral depth was arbitrarily fixed at 15 km depth (with a 10 km depth also tested), to be consistent with the present-day seismogenic depth and with the extent of the 1887 macroseismic observations (matched by a focal depth between 10 and 20 km). Starting from these assumptions, we tested a wide range of earthquake source scenarios. Given the Plio-Quaternary and the present-day deformation of the margin (Larroque *et al.* 2011b), the preferred scenario is a predominantly reverse faulting mechanism along a N60°–70°E fault plane dipping to the north. However, because the faulting mechanism of the 1887 earthquake is not fully established, we tested other possibilities: (i) a pure reverse faulting along a south-dipping plane, which could correspond to a possible inversion of one of the normal faults inherited from the Oligo-Miocene rifting (Larroque & Sage 2011) and (ii) the reactivation of one of these inherited faults by pure normal faulting. We should note that this last possibility remains theoretical because normal faulting on such a structure is not consistent with the present-day regional state of stress (Béthoux *et al.* 1992; Eva & Solarino 1998; Baroux *et al.* 2001; Larroque *et al.* 2009).

For each scenario we tested a coseismic slip consistent with our macroseismic results: ranging from 0.8 to 1.5 m, which corresponds to a magnitude M_w of 6.5–6.9, respectively, and a rupture length in the range of 20–40 km, respectively (Wells & Coppersmith 1994). Taking into account the distribution of the maximum run-ups (Fig. 5), we propose that mainly the eastern part of the LFS was ruptured (Fig. 6).

TSUNAMI MODELLING

The numerical modelling procedure

We used the FUNWAVE tsunami propagation and run-up/inundation model. The model is fully non-linear and dispersive, while retaining information to the leading order in frequency dispersion $O[(kh)^2]$ and to all orders in non-linearity a/h (where k denotes an inverse wavelength scale, a denotes a wave amplitude and h denotes a water depth; Wie & Kirby 1995; Wie *et al.* 1995). The model treats the entire computational domain as an active fluid domain by using an improved version of the slot or permeable-seabed technique; that is, the moving shore-line algorithm proposed by Chen *et al.* (2000) and Kennedy *et al.* (2000) for the simulation of run-up. The model includes bottom friction

and energy dissipation to account for the wave breaking, and a subgrid turbulence scheme. The model has already been validated for various earthquake/tsunami events (Ioualalen 2008; Ioualalen *et al.* 2006, 2007, 2010a,b; Ilayaraja *et al.* 2008; Mard Karisson *et al.* 2009). In relation to this study, for the 2004 December 26, Indian Ocean earthquake/ tsunami, Ioualalen *et al.* (2007) calibrated a seismic source mainly from hydrographic records (tide gauges) that turned out to be relatively accurate. Based on these results and their methodology, we expect that the hydrodynamic information (here the simulated tsunamis for the different scenarios) will provide us with some information on the 1887 rupture characteristics, and may eventually allow us to identify a coherent scenario. The initial wave is computed from the Okada dislocation model (1985). The rupture characteristics proposed in our scenarios included fault geometry, focal depth, fault plane centroid location and amount of slip; these were input into the model, and an initial tsunami was generated, providing its source properties (characteristic initial wave length and period, initial trough and peak amplitudes).

The bathymetry was derived from different sources, including multibeam bathymetric surveys operated by IFREMER (Institut Français d'Exploration de la Mer) in the basin and the continental margin, and by the SHOM (the French Service Hydrographique et Océanographique de la Marine) for the coastal area, with 25–50 m resolution. Fifty-metre resolution data was obtained from IGN (the French Institut Géographique National) and used for the land topography.

We constructed a 200-m-grid-spacing computational domain that covered a region from 43°05'N to 44°27'N, and from 6°32'E to 9°15'E (1150 × 776 grid nodes). A 0.25 s optimal time step was chosen to avoid numerical instabilities and truncation errors. A propagation time of 55 min has been chosen (13 200 time steps) to simulate the first three to four wave crests, for validation against the Genoa tide record. We found that it was not worth running a longer propagation. This is because the first crests are directly related to the source characteristics (convoluted with site effects), while the following crests are more exclusively related to site effects, which is not our interest here. Our version of the FUNWAVE tsunami propagation model does not allow subdomains. Considering that hundreds of numerical simulations needed to be performed for this study, we could not use a more accurate grid.

The Genoa tide gauge processing

For this event, the tide gauge records of Genoa and Nice harbour are available (Eva & Rabinovich 1997). However, the record in Nice cannot be exploited because of a sudden drop in the sea level that is difficult to explain and thus to model. We thus focussed on the Genoa record for the following.

A low-pass Hanning filter was applied to the tide gauge signal (periods lower than 2400 s are filtered; Fig. 7). Then the residual was extracted (initial signal–low-pass signal). The 2400 s filtering-period was chosen so that it is relatively far from the tide diurnal and semi-diurnal periods, and also from the approximately 700–800 s of the tsunami period. We could not remove the low-amplitude oscillations (±4 cm) of periods of 600–700 s that were present prior to the tsunami arrival, because these are close to the tsunami period (e.g. at the earthquake occurrence time in Fig. 7). These nonfiltered oscillations probably explain the distortion of the processed tsunami signal. We also wanted to keep any potential dispersive effects in the tsunami component of the recorded wave. These oscillations might be associated with the resonance frequency of the harbour (Eva & Rabinovich 1997), which we resolved in our 55 min time window of propagation (discussed later). As it was not possible

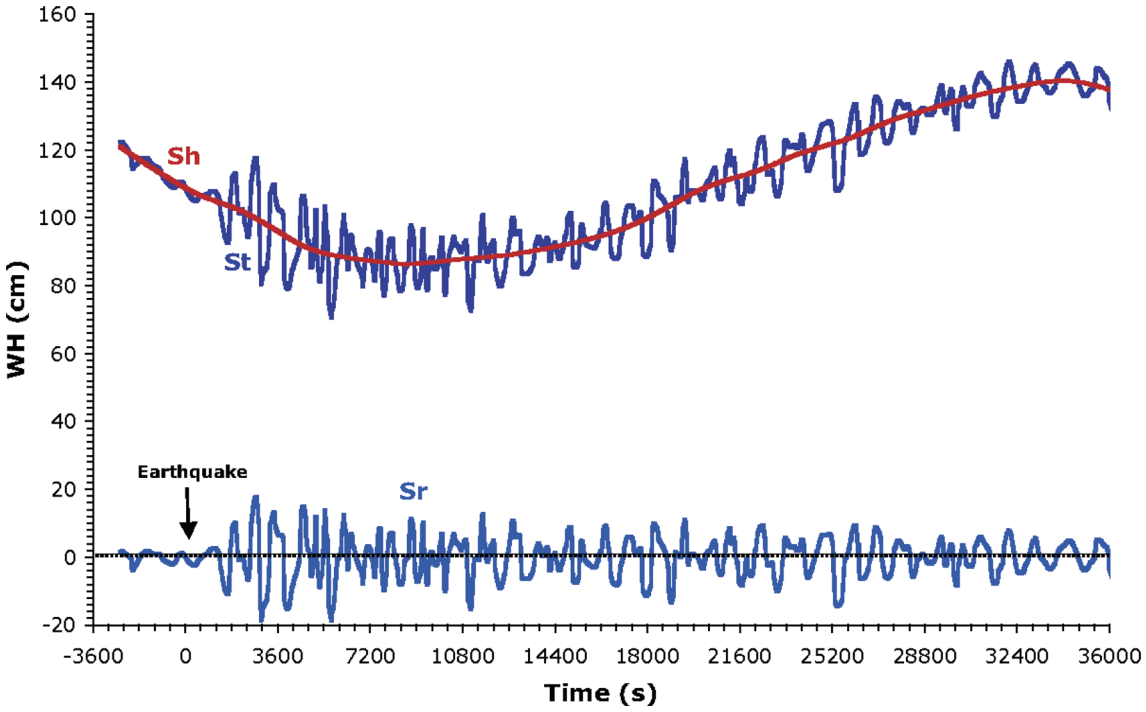

Figure 7. Tide gauge record digitalized from Eva & Rabinovich (1997) (St for 'Signal-total', dark blue). The approximate tidal signal was obtained from a 2400 s period low-pass Hanning filter (Sh for 'Signal-hanning', red). The tide residual Sr (Sr for 'Signal-residual', blue) is obtained through St-Sh. The time is in seconds and the water wave height (WH) is in cm. The vertical arrow indicates the time occurrence of the earthquake based on the tide gauge clock (6 hr 21 min Genoa local time, from Eva & Rabinovich 1997; 5 hr 22 min GMT, from Guidoboni *et al.* 2007), set here to $t = 0$.

to filter these oscillations, the only way to remove them would have been to predict them (and then remove them) through, for example, a bootstrap technique. However, we cannot rely on such a procedure, as it would certainly downgrade the tsunami component of the record. In our study, we kept this 3–4 cm wave amplitude uncertainty in mind, along with a possible tsunami phase shift. This difficulty to completely (and correctly) isolate the tsunami signal is of primary importance in our study, and it will be crucial in the potential conclusions while identifying the best-fitting earthquake kinematics.

As far as the earthquake time of occurrence is concerned (set to $t = 0$; Fig. 7), Eva & Rabinovich (1997) reported it as 6 hr 21 min local time in Genoa. There is unavoidably, however, uncertainty associated with the tide gauge clock. Any possible processing of the phase and amplitude of the predicted tide (which is not accurate) to fix a time reference carries the risk of introducing an error that would, for example, constrain the epicentre location too much. Instead of introducing such a possible error in the location, we preferred to remove the reference time constraint. Consequently, we preferred not to use the tsunami arrival time to constrain our scenarios. Rather, we made the choice to impose a time lag/shift on the simulated signal of our multiple scenarios by using, as an arbitrary criterion, the optimal time associated with the optimal cross-correlation between the recorded and the simulated signals. This criterion is not entirely satisfactory, but we proceeded in this way in this study.

Analysis of the tide gauge record and the simulated signal at Genoa

All of the rupture parameters tested are given in Table 3. First, a strike angle of N70°E was tested, in agreement with the above morphotectonic analysis. We, however, moved from this value to optimize a solution consistent with the tsunami. Based on the present-day seismicity (Courboulex *et al.* 2007; Larroque *et al.* 2009), this analysis consider a rake range from 74° to 116°. These rakes were tested for all of strike scenarios, and they were found not to change the wave amplitude and sequence significantly. We then kept the pure thrust and normal faulting configuration (rake of 90°).

For a strike angle of N70°E, a 40 × 15 km size for the rupture plane (40 km along the strike, and 15 km in the transverse direction) led to an optimal fit of the signal. Alternative sizes were also tested (50 × 12 km and 30 × 20 km), but these are not shown here because they yielded a relatively too-large trough at around 2800 s. For this configuration, within this range of 'allowed' fault-size, there was no significant change on the tsunami period which would have provided an interesting parameter for 'calibrating' the fault parameters. For the same reason, a 15-km-focal depth was chosen (10 km was also tested). Subsequently, we tested different amounts of slip, from 0.8 m associated with M_w 6.5 (and a surface faulting of 20 km × 15 km), which produced too weak a signal (e.g. simulation S1 in Table 3, for the case of a reverse fault dipping towards the south; Fig. 8), up to 1.5 m associated with M_w 6.9, which closely reproduced the wave amplitude.

Table 3. Scenarios discussed in the text for the 1887 event corresponding to variation in the parameters of the Okada (1985) dislocation method, with each one corresponding to a specific rectangular ruptured area. For these scenarios, the centroid location is kept constant (8.07°E, 43.70°N) and the centroid focal depth d is fixed at 15 km. L is the length along the strike of the rectangular fault plane, and W is the width transverse to the fault plane. ϕ and δ are the strike and dip angles, respectively. The rake angle λ is kept constant (90°). Δ is the co-seismic slip. The medium shear modulus is taken as $\mu = 4 \times 10^{10}$ Pa. M_w is the corresponding seismic moment.

Scenario	Kinematics	Strike	δ (dip)	L (km)	W (km)	Δ (m)	M_w
S1	Reverse	N70°E	70°S	20	15	0.8	6.5
S2	Normal	N70°E	70°N	40	15	1.5	6.9
S3	Normal	N70°E	70°S	40	15	1.5	6.9
S4	Reverse	N70°E	74°S	40	15	1.5	6.9
S5	Reverse	N70°E	16°N	40	15	1.5	6.9
S6	Reverse	N55°E	74°S	35	17	1.3	6.8
S7	Reverse	N55°E	16°N	35	17	1.5	6.9

We considered the entire set of possible kinematics; for example, reverse or normal faulting along planes dipping towards the south or the north. Independent of the considered rupture parameters (dip, rake and strike angles, amount of slip, size of rupture plane), the normal faulting scenarios yielded a leading trough of the tsunami that was not consistent with the Genoa tide gauge record (S2 and S3 in Table 3 and Fig. 8).

On the contrary, both reverse faulting kinematics along north-dipping or south-dipping fault planes showed a coherent leading crest (see below). The remaining parameter, that is, the dip angle, was found to be optimal for a fault plane dipping 74° towards the south or 16° towards the north (S4 and S5 in Table 3 and Fig. 9). Bearing in mind the systematic potential error of the tide gauge clock, the first issue was to (arbitrarily) synchronize the tide gauge record and the simulation result by matching their respective optimal cross-correlations to correspond both to a 410-s shift of the simulated time series. For the south-dipping fault plane, a high dip angle (>74°) tended to increase the wave amplitude, while a low dip angle did not resolve the double peak. We observed the contrary for the north-dipping fault plane (S5 in Table 3). Also, to extract the best-fitting solutions, we focussed on the large (second) trough and (third) peak because they were less sensitive to our 3–4 cm of uncertainty. With these best-fitting reverse faulting solutions, we reproduced the entire signal following the first crest (after $t =$ 2100 s) coherently in amplitude and phase. In particular, the double peak centred at $t = 2300$ s is resolved as well as the following large trough and crests. The first crest is reproduced in amplitude, but with a phase lag that can be partly explained by the 3–4 cm amplitude and associated phase uncertainties. The amplitude of the first trough is also not correctly modelled, but this time, the 3–4 cm of uncertainty cannot explain the difference (in the order of 10 cm).

We have computed various statistics (Table 4) to evaluate the plausibility of the source. The statistics were performed for the time window ranging from the initiation of the leading trough ($t_0 =$ 1350 s after the presumed earthquake occurrence, based on the tide gauge clock in Fig. 7) to the end of the third trough ($t_{end} = 3300$ s; Fig. 9). With this relatively short time window, we hoped to capture the main initial wave.

The respective simulated amplitudes and frequency content are described in terms of objective basic fit statistics and the wave spectrum. Our solutions S4 and S5 show relatively satisfactory 0.69 and 0.65 cross-correlation coefficients (Table 4). Thus the respective mean wave heights (0.97 and 0.08 cm) lie within our ±3–4 cm range of uncertainty, and the standard deviations (8.95 and 9.27 cm) are comparable. The relatively poor RMSE can be partly explained by the 3–4 cm of uncertainty and the poor recovery of the first trough phase. Qualitatively, we can always find a correct superimposition (at least linearly) of a 3–4 cm wave height signal for our simulated tsunami, and substantially improve the shape of the first crest and the statistics (more difficult for the first through).

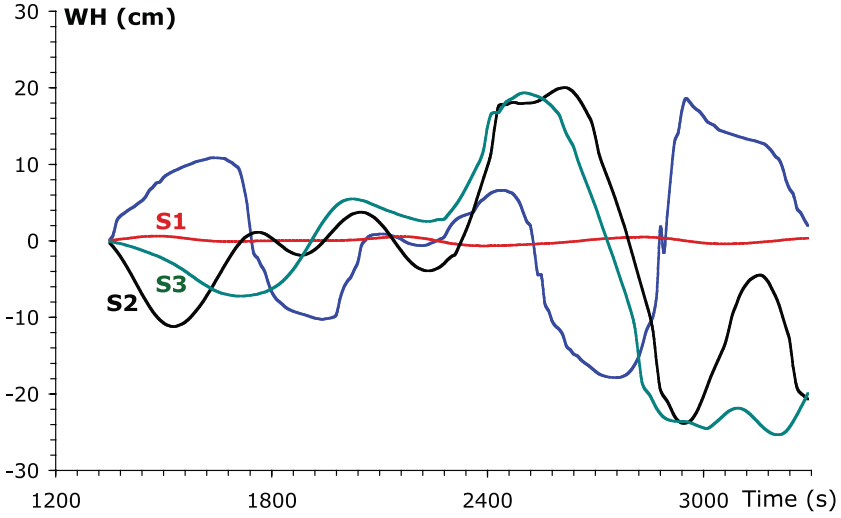

Figure 8. Comparison between the Genoa tide gauge record (blue) and the simulated time series for scenarios S1 (red), S2 (black) and S3 (green) of Table 3. Time is in seconds, and the wave height (WH) is in cm. Here we have shifted the tsunami signals to match the recorded tide gauge signal arrival time.

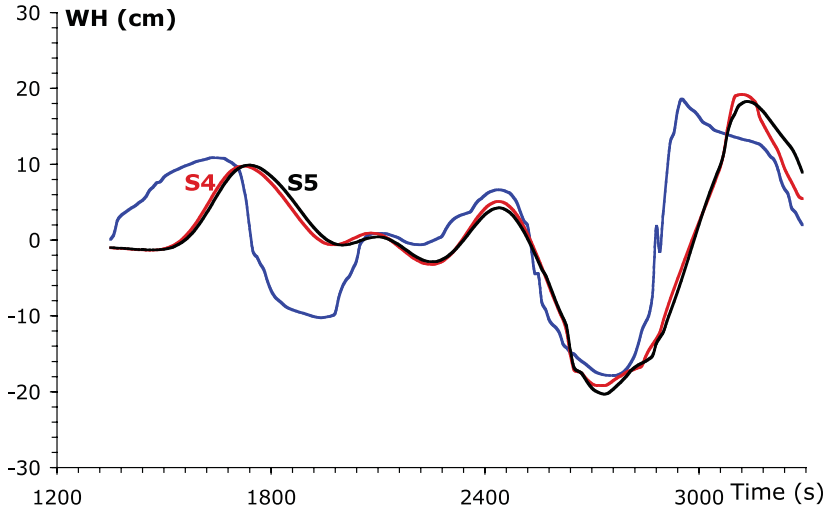

Figure 9. As for Fig. 8, for scenarios S4 (red) and S5 (black) of Table 3.

Table 4. Statistics of the match between the Genoa tide gauge record (index $_{\mathrm{Rec}}$) and our best-fitting solutions, of models S4, S5, S6 and S7 of Table 3 (index $_{\mathrm{Sol}}$). The basic statistics are the mean wave height $\bar{\eta}$, the standard deviation σ, the root mean squared error (RMSE) ε, and the cross-correlation coefficient ρ. The usual RMSE represents the model skill and is defined as $\sqrt{\sum_i (\eta_{\mathrm{Rec}} - \eta_{\mathrm{Sol}})^2 / n}$, where η_{Rec} corresponds to the tide gauge record points, η_{Sol} to the associated simulated points and n is 195 (number of comparison points from 1330 to 3290 s, every 10 s).

	$\bar{\eta}_{\mathrm{Rec}}$ (cm)	$\bar{\eta}_{\mathrm{Sol}}$ (cm)	σ_{Rec} (cm)	σ_{Sol} (cm)	ε (cm)	ρ
S4	1.05	0.97	9.78	8.95	7.49	0.69
S5		0.08		9.27	8.04	0.65
S6		1.14		8.70	6.14	0.79
S7		1.52		9.51	6.32	0.79

The spectrum resolution makes its evaluation tenuous, because only a few periods can be computed around the dominant 513 s peak of the tide gauge (Fig. 10). The tide gauge record has two main peaks, at 513 and 320 s, which differ from the scenarios S4 and S5: 640 and 233 s (spectrum S4 is not shown as it is quasi-identical to that of S5). This indicates that the wave sequence (the successive phase and amplitudes of the crests and troughs) is not well resolved.

At this stage, we attempt to improve the recovery of the first wave trough amplitude and the frequency content. With the proposed weak dip angles (16°, close to 0°, for the north-dipping fault plane, and 74°, close to 90°, for the south-dipping one), the first crest/ trough asymmetry (with crest amplitude much higher than trough amplitude) is due to the wave directivity. A way to reduce this asymmetry is to rotate the rupture plane counter-clockwise; for example, by lowering the strike angle from N70°E (tested from N0° to N60°E; not shown). We found an optimal strike angle of N55°E (S6 and S7 in Table 3). This value remains close to the N60°E–N70°E orientation of the shallow traces of the active faults and it is therefore consistent with the geometry of the LFS. This time (Fig. 11), we recovered both the first peak and the trough within our 3–4 cm of uncertainty (only 4 cm difference for the trough). The statistics were improved (Table 4), with an excellent 0.79 cross-correlation

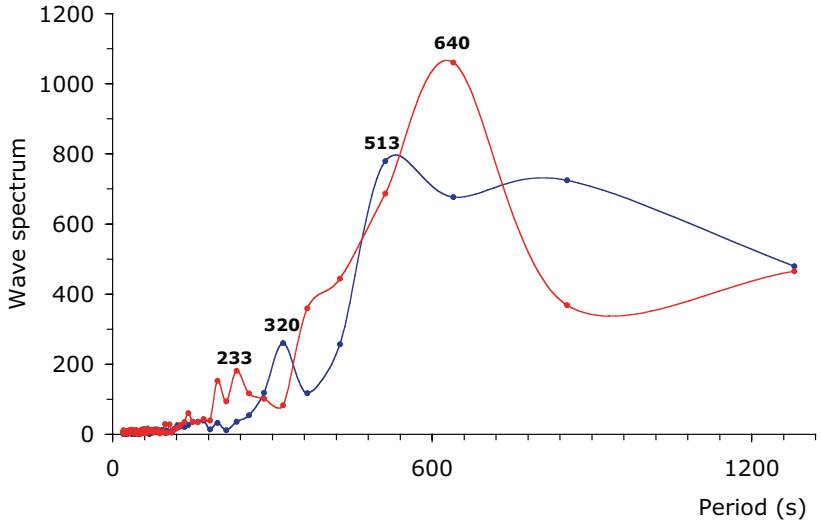

Figure 10. Wave spectra comparison between the Genoa tide gauge record (blue) and scenario S5 (red) of Table 3.

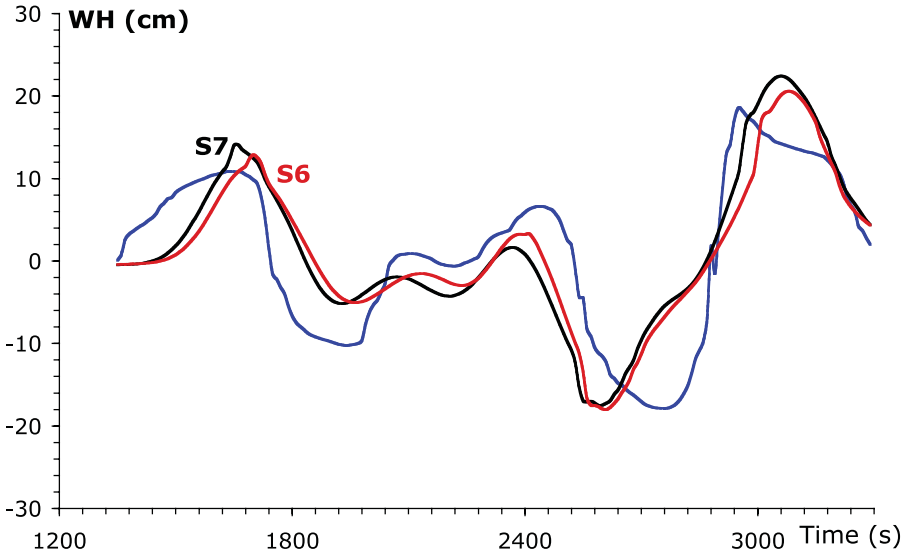

Figure 11. As for Fig. 8 for scenarios S6 (red) and S7 (black) of Table 3.

coefficient for both scenarios. This means that the standard deviations and RMSEs lie within our 3–4 cm of uncertainty. Furthermore, the wave spectra for S6 and S7 (spectrum S6 not shown because it is almost identical to that of S7) indicate very good matches of the frequency content (Fig. 12).

Eva & Rabinovich (1997) computed the wave spectrum of the Genoa tide gauge before and during the tsunami. In both cases, they found an approximately 22.5-min peak and (lower period) 9-min and 5.9-min harmonics, which they attributed to the harbour resonance periods. With our total wave propagation time of 55 min and an arrival time of 22 min at the gauge, there are 33 min of the wave train modelled. Consequently, for our wave spectra computed in Fig. 12, we resolved only the periods shorter than $33/2 = 16.5$ min. This range comprises their harmonics of 9 and 5.9 min. Here we obtained very good fit (see Fig. 12 for 513 and 320 s). For their 22.5-min period, we do not resolve this in the wave spectra computation, but the arrival of this resonance wave was included within our 33-min propagation window, and thus this is intrinsically included in the fit statistics of Table 4. The initial waves were set as equivalent to the vertical seafloor coseismic deformation, and they are shown in Fig. 6.

DISCUSSION

Tsunamis most commonly arise from earthquakes and/or submarine landslides (e.g. Fryer *et al.* 2004; McAdoo & Watts 2004; von Huene *et al.* 2004; Bliek 2009; Ioualalen *et al.* 2010c). As a great number of submarine failures of various sizes have been identified along the northern Ligurian margin (Migeon *et al.* 2011), the origin of the 1887 February 23, tsunami remains uncertain. In the epicentral area, from high-resolution bathymetry and core dating, Hassoun *et al.* (2009) have identified submarine failures in the time window of the Ligurian earthquake. However, the maximum volume involved in these submarine slides was in the range of 0.005 km^3 and as such appears too small to trigger a tsunami with the observed extent and run-up characteristics (Ioualalen *et al.* 2010c). Therefore,

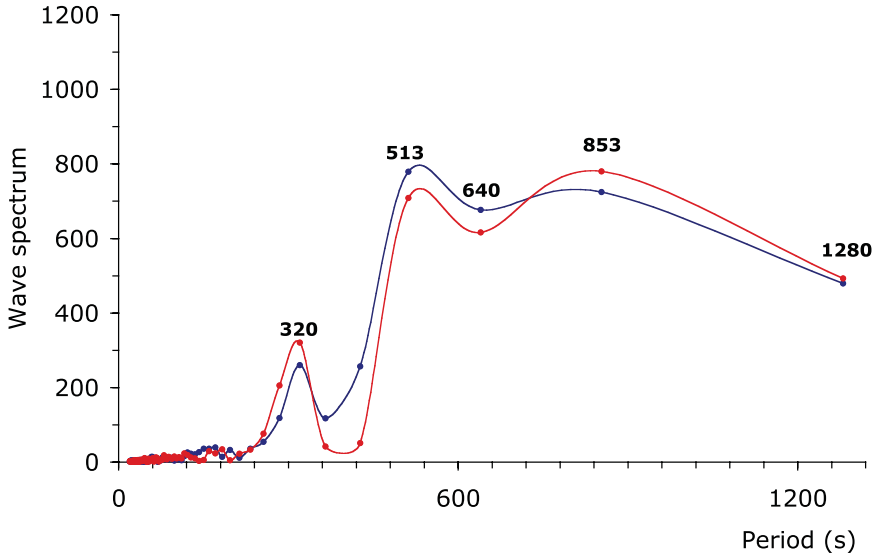

Figure 12. Wave spectra comparison between the Genoa tide gauge record (blue) and scenario S7 (red) of Table 3.

we only support the origin of the earthquake-induced tsunami for the 1887 Ligurian event, and the submarine slides hypothesis was rejected.

From the two macroseismic data sets (SISFRANCE-08 and DBMI-04) and using the Provence attenuation model of Bakun & Scotti (2006), the location of the 1887 earthquake is found to be off-shore Imperia and the hypocentre to be consistent with a location 10–20 km depth below the northern Ligurian margin (Table 2). The assessment of the macroseismic moment magnitude gives a wide interval between 6.3 and 7.5 (Table 2), which is consistent with the length and geometry of active faults revealed along the northern Ligurian margin. In any case, all location estimates agree with the faulting of a structure located off-shore and dipping to the north, such as the LFS (Fig. 13).

One important question remains: did the 1887 earthquake break the surface? No trace of surface rupture directly related to this earthquake was found during the MALISAR geophysical surveys (Larroque *et al.* 2011b). Even though crustal earthquakes of $M_w >$ 6.5 do not necessarily break the surface (e.g. Triep *et al.* 1995; Arjannikova *et al.* 2004), the question remains open because the current resolution of our bathymetric data are certainly too low to identify offsets in the range of 1 m. It has now been demonstrated that advanced marine imaging and dating methods allow fault characterization (slip rate, length, segmentation and kinematics; e.g. Nodder *et al.* 2007; Lamarche *et al.* 2011) and identification of coseismic ruptures at the sea floor. As the Ligurian earthquake was a major seismic and tsunami event in the region, it warrants to be further investigated.

From the tsunami modelling, and based on the seismotectonic analysis, we think that the most pertinent scenarios have been tested by considering a coseismic slip in the range of 0.8–1.5 m and a focal depth of 15 km. Regarding the kinematics and the geometry of the fault, the two best-fitting solutions appear to be reverse faulting along a N55°E fault plane either dipping towards the south by 70° or towards the north by 16°. From simple fit statistics, these scenarios are the most consistent with the tide gauge record of Genoa. We note that the N55°E strike is mainly consistent with the mean strike of the eastern LFS and the activation of the eastern part of the LFS is in accordance with the distribution of the maximum run-ups near Imperia (Fig. 5).

It is interesting to note the similarity between the two reverse faulting solutions. Whatever the rupture kinematics, the Okada (1985) solution shows a dipole uplift/ subsidence of the seafloor deformation across-strike (crest/trough for the initial wave), which evolves with the dip angle: around a given critical dip angle, the dipole reverses (Ioualalen 2009). For the same dip angle, the two dipoles for the north-dipping and south-dipping fault plane are opposite, while for a high south-dipping fault plane (close to 70°) and for a low north-dipping fault plane (close to 20°) the dipoles are very similar. This non-uniqueness of the deformation solution explains the similarity between the initial waves of the S6 and S7 scenarios (Figs 6 and 11; idem for S4 and S5). Therefore, we must take into account additional information to determine the best scenario.

Following these hypotheses, the vertical seafloor coseismic deformations were computed from the Okada dislocation model (Fig. 6): this corresponds to a subsidence of around 5–10 cm along the coast from San Remo to Albenga (Fig. 6). Unfortunately, no data related to possible subsidence/uplift was collected along the coast just after the 1887 event. For the long-term tectonics, recent studies have revealed the overall uplift of the margin, as follows.

(i) Several morphotectonic characteristics (shape of the drainage network, fault scarps, strong slope gradient) attest to the Quaternary uplift of the continental slope off-shore of Imperia (Imperia Promontory, Fig. 2), and this uplift was generated by the reverse faults that bound the southern edge of the promontory. Clearly, the uplift of the northern Ligurian margin is the response to a long-term compressional deformation that started after the Messinian times (5.3 Myr), and that has continuously been active, as shown by the faulted and folded Quaternary deposits (Mercier de Lépinay *et al*. 2007). The long-term uplift rate is proposed to be in the range of 0.40–0.53 mm yr^{-1} for the Plio-Quaternary times. This is a significant value in such a low deformation rate area (Larroque et al. 2011b).

(ii) Onshore, Federici & Pappalardo (2006) and Dubar et al. (2008) suggested the Holocene uplift of the French Riviera and the Ligurian coast from analysis and new radiometric dating of marine terraces. This deformation is also consistent with reverse faulting along north-dipping fault planes located off-shore.

On the other hand, as discussed previously, the northern Ligurian margin shows a strong tectonic inheritance that is related

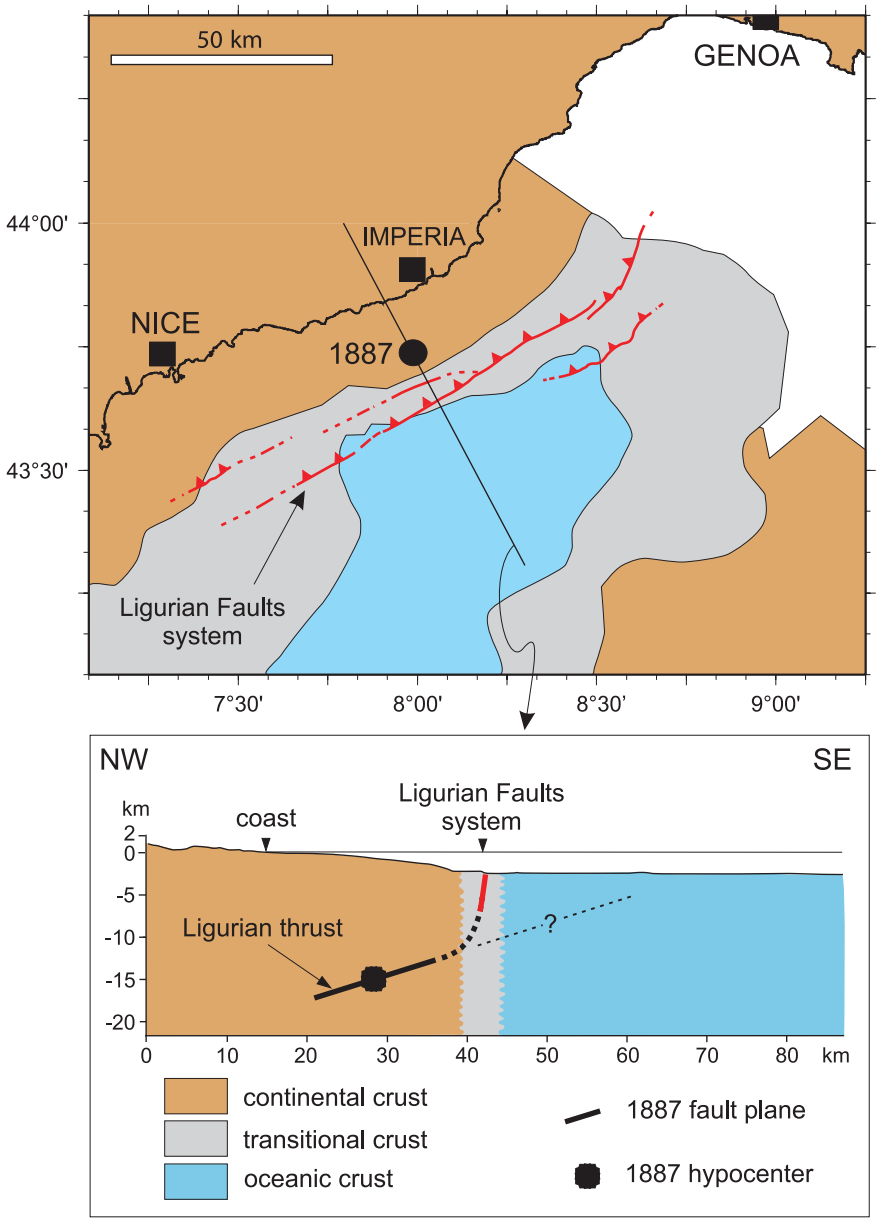

Figure 13. Seismotectonic sketch of the 1887 Ligurian earthquake. The 1887 hypocentre is located along the northward low-dip Ligurian thrust (our preferred solution). The Ligurian thrust could be connected to the Ligurian Faults system at shallow depth (red). The narrow dotted line represents the possible continuation of the Ligurian thrust towards the south. The boundaries between the continental, transitional and oceanic crust are taken from Rollet *et al.* 2002), the white domain is certainly of continental crust type.

to the Oligocene–Miocene rifting process (e.g. Réhault *et al.* 1984; Rollet *et al.* 2002). These old large normal faults dipping towards the south might be reactivated in the recent compressive context. This is the reason for the discussion of the scenarios S1, S4 and S6. However, despite a careful structural investigation, no inversion of the south-dipping normal faults was seen from the seismic imagery of the margin (Sage *et al.* 2011; Larroque & Sage 2011), and furthermore, no morphotectonic traces were identified for uplift along the southern continental slope (Larroque *et al.* 2011b). It appears that the major structures that can accommodate the present-day deformation are only the north-dipping faults.

At depth, the low dip of the fault (16°) is in favour of a flat thrust below the northern Ligurian margin. Therefore, from: (1) the macroseismic data; (2) the tsunami modeling; (3) the active deformation and (4) the long-term tectonics, we propose the activation of this major N55°E striking thrust by an earthquake of M_w 6.9 with a dominantly reverse faulting kinematics as the most consistent scenario to account for the 1887 Ligurian earthquake.

The deep-seated geometry of such a major thrust is currently unknown, although the geometry and the Quaternary compressional activity of the LFS suggest that they are connected (Fig. 13). The emergence of this major thrust plane at the foot of the Ligurian margin may be controlled by changes in the rheology in the ocean–continent transition zone (Béthoux *et al.* 2008). Therefore, we favour the idea the 1887 rupture might have been propagated from the Ligurian thrust through the LFS and might have reached the oceanic floor (Fig. 13). Nevertheless, as significant compressional deformation occurs further southwards (e.g. 1963 July 19; M_L 6.0; Fig. 1), it cannot be excluded that the low-dip Ligurian thrust propagates towards the south (Fig. 13).

The Ligurian earthquake appears to be significant for this area, considering the relatively low extent of the active faults (compared to the great subduction areas; e.g. Ioualalen *et al.* 2007, for the 2004 Sumatra event). As a result, this event might represent a worst-case scenario in terms of the tsunami impact for the Ligurian coast, and the associated hazard must be detailed (work in progress).

CONCLUSIONS

This reappraisal of this 1887 Ligurian event is based on: (i) the new morphotectonic data acquired on the northern Ligurian margin; (ii) the French and Italian data sets of intensity assignments, combined with the Provence intensity attenuation model proposed by Bakun & Scotti (2006) and (iii) tsunami modelling tested against the record of the Genoa tide gauge. We have obtained a better assessment of the possible seismic source, and we detail the likely geometry of the active fault, the kinematics of the faulting, and the coseismic slip. We must be cautious about our analysis, as the tectonic, macroseismic and tsunami data are not complete; nevertheless, the fact that our proposed scenario can reconcile the different data strengthens our interpretations.

The recently identified LFS is an 80-km-long segmented active fault that runs along the foot of the continental slope. Our results show that the epicentral location and the magnitude of the 1887 event differ slightly according to the Italian and the French data sets. Despite this, both data sets are consistent with the epicentral location at sea (off-shore of Imperia), at 10–30 km from the coast, assuming a focal depth in the range of 10–20 km. The inferred magnitude range was $6.8 < M_w < 7.5$ and $6.3 < M_w < 6.9$, for the French and Italian data sets, respectively.

From the extent and the amplitude of the tsunami waves, we ruled out the hypothesis of a submarine-landslide source, and we considered that the Ligurian earthquake triggered the tsunami. From the distribution of the run-ups, we considered that mainly the eastern part of the LFS was ruptured. Numerous seismic scenarios (rupture parameters: fault length, fault dip, rake angle and coseismic slip) were tested against hydrographic data by performing tsunami model. The scenarios that are consistent with the Genoa tide gauge require a N55°E striking fault with a 35-km-long and a 17-km-wide fault, with a hypocentral depth of 15 km and a reverse coseismic displacement of 1.3–1.5 m. This leads to the refinement of the magnitude of the earthquake to M_w from 6.8 to 6.9, in the upper range of the macroseismic analysis results. The optimal solutions are reverse faulting along a plane dipping 70° towards the south or 16° towards the north. Taking into account the tectonic data, we favour the hypothesis of the northward dip for the active fault. Therefore, our proposal for the 1887 earthquake is the activation of a 35-km-long, 17-km-wide and N55°E striking fault, dipping 16° to the north, with a coseismic slip of 1.5 m, and a focal depth of 15 km.

This study was designed to characterize the major historical event in the south-western Alps–Ligurian Basin area by taking into account all of the available data. The result provides better understanding of underwater earthquakes and tsunamis, in order to define the hazards for the significant population in this coastal area. This preliminary analysis raises two important questions: (i) as the morphotectonic features show that the long-term deformation of the LFS can correspond to an accumulation of displacements from repeated earthquakes, such as the 1887 one, we should try to further highlight the long-term history of this fault by characterizing the recurrence time of such earthquakes and tsunamis and (ii) as we define several potential seismic source scenarios that are significant for this area, there remains the need to investigate the consecutive wave height distributions and the associated tsunami hazards (work in progress).

ACKNOWLEDGMENTS

The authors thank André Laurenti for discussions about the history of the 1887 Ligurian earthquake/tsunami and for providing us with the map of Fig. 5. G. Capponi and E. Eva kindly, although unsuccessfully, helped us to recover the original Genoa tide gauge. Bertrand Delouis discussed the dislocation model with us. This work was funded by the Agence Nationale de la Recherche through the ANR projects QSHA ('Quantitative Seismic Hazard Assessment', http://qsha.unice.fr/) TSUMOD (ANR-05-CATT-016–02), and by the project 'sismicité de l'hexagone' (CNRS-CEA-MEDDTL, convention no. 2100474508). The MALISAR geophysical surveys of the northern Ligurian margin were funded by the Commission Nationale Flotte et Engins (CNFE-IFREMER). We thank Stephano Solarino, Saskia Goes (editor) and an anonymous reviewer who provided interesting comments and suggestions.

REFERENCES

Ambraseys, N.N., 1962. Data for the investigation of seismic sea waves in the Eastern Mediterranean, *Bull. seism. Soc. Am.,* **52,** 895–913.

Arjannikova, A., Larroque, C., Ritz, J.F., Déverchère J., Stéphan J.F., Arjannikov S. & San'kov, V., 2004. Geometry and kinematics of recent deformation in the southwesternmost Baikal rift zone (Mongolia-Siberia), *Terra Nova,* **16,** 265–272.

Augliera, P., Béthoux, N., Déverchère, J. & Eva, C., 1994. The Ligurian Sea: new seismotectonic evidence, *Bolletino di Geofisica Teorica e Applicata,* **XXXVI**(141–144), 363–380.

Bakun, W.H. & Wentworth, C.M., 1997. Estimating earthquake location and magnitude from seismic intensity data, *Bull. seism. Soc. Am.,* **87**(6), 1502–1521.

Bakun, W.H. & Hopper, M.G., 2004. Magnitudes and locations of the 1811–1812 New Madrid, Missouri, and the 1886 Charleston, South Caroline Earthquakes, *Bull. seism. Soc. Am.,* **94**(1), 64–75.

Bakun, W.H. & Scotti, O., 2006. Regional intensity attenuation models for France and the estimation of magnitude and location of historical earthquakes, *Geophys. J. Int.,* **164,** 596–610.

Baroux, E., Béthoux, N. & Bellier, O., 2001. Analyses of the stress field in the southeastern France from earthquake focal mechanisms, *Geophys. J. Int.,* **145,** 336–348.

Basili, R., Valensise, G., Vannoli, P., Burrato, P., Fracassi, U., Mariano, S., Tiberti, M.M. & Boschi, E., 2008. The Database of Individual Seismogenic Sources (DISS), version 3: summarizing 20 years of research on Italy's earthquake geology, *Tectonophysics,* **453,** 20–43.

Béthoux, N., 1992. Mécanismes au foyer et néotectonique: application à la mer Ligure (Méditerranée occidentale), *Quaternaire,* **3,** 97–104.

Béthoux, N., Fréchet, J., Guyoton, F., Thouvenot, F., Cattaneo, M., Eva, C., Nicolas, M. & Granet, M., 1992. A closing Ligurian sea, *Pure appl. Geophys.,* **139,** 179–194.

Béthoux, N., Sue, C., Paul, A., Virieux, J., Fréchet, J., Thouvenot, F. & Cattaneo, M., 2007. Local tomography and focal mechanisms in the south-western Alps : comparison of methodes and tectonic implications, *Tectonophysics,* **432,** 1–19.

Béthoux, N., Tric, E., Chery, J. & Beslier, M.O, 2008. Why is the Ligurian basin (Mediterranean sea) seismogenic? Thermomechanical modelling of a reactivated passive margin, *Tectonics,* **27,** TC5011, doi:10.1029/2007TC002232.

Bianchi, A., 1888. Terremoti del febbraio 1887 nella Liguria orientale, *Rivista Meteorico-Sismica per gli anni 1885–86 e 1886–87,* Tipografia-Lithografia G. Esposito, Chiavari.

Bigot-Cormier, F., Sage, F., Sosson, M., Déverchère, J., Ferrandini, M., Guennoc, P., Popoff, M. & Stéphan, J.F., 2004. Déformations pliocènes de la marge nord-Ligure (France): Les conséquences d'un chevauchement crustal sud-alpin, *Bulletin de la Société Géologique de France,* **175**(2), 197–211.

Bliek, S.L., 2009. Seismicity along the South American subduction zone: review of large earthquakes, tusnamis, and subduction zone complexity, *Tectonophysics,* doi:10.1016/j.tecto.2009.02.037.

Boschi, E., Ferrari, G., Gasperini, P., Guidoboni, E., Smriglio, G. & Valensise, G., 1995. *Catalogo dei forti terremoti in Italia dal 461 A.C. al 1980,* p. 973, Istituto Nazionale di Geofisica-Storia Geofisica Ambiente, Bologna.

Bossolasco, M., Cicconi, G., Eva, C. & Pascale V., 1972. La rete sismica dell'Istituto Geofisico di Genova e primi risultati sulla sismo-tettonica delle Alpi Marittime ed Occidentali, e del Mar Ligure, *Rivista Italiana di Geofisica,* **XXI**(5/6), 229–247.

Camelbeeck, T., Galadini, F., Meghraoui, M. & van den Berg M., 2001. Evaluation of the potential for large earthquakes in regions of present-day low seismic activity in Europe, *Neth. J. Geosci.– Geologie en Mijnbouw,* **80,** 67–68.

Chamoot-Rooke, N., Gaulier, J.M. & Jestin, F., 1999. Constraints on Moho depth and crustal thickness in the Liguro-Provençal basin from 3D gravity inversion : geodynamic implications, in *The Mediterranean Basins: Tertiary extension within the Alpine orogen,* Geol. Soc. Lond. Spec. Pub. Vol. 156, pp. 37–62, eds Durand, B. *et al*., Geological Society, London.

Chaumillon, E., Déverchère, J., Réhault, J.P. & Gueguen, E., 1994. Réactivation tectonique et flexure de la marge continentale Ligure (Méditerranée Occidentale), *Comptes Rendus de l'Académie des Sciences de Paris,* **319,** 675–682.

Capponi, G., Cattaneo, M. & Merlanti, F., 1985. The Ligurian earthquake of February 23, 1887, in *Atlas of Isoseismal Maps of Italian Earthquakes,* pp. 100–103, ed. Postpischl, D., CNR-PFG, Quaderni de la Ricerca Scientifica, 114 2A, Consiglio Nazionale delle Ricerche, Roma.

Chen, Q., Kirby, J.T., Dalrymple, R.A., Kennedy, A.B. & Chawla, A., 2000. Boussinesq modelling of wave transformation, breaking, and run-up. II: 2D, *J. Waterway, Port, Coastal, Ocean. Eng.,* **126,** 48–56.

Cobbold P., 2008. Horizontal compression and stress concentration at passive margins: causes, consequences, and episodicity, in *Proceedings of the 33rd International Geological Congress,* Oslo, August 6–14, http://www.cprm.gov.br/33IGC/1323276.html.

Contrucci, I., Nercessian, A., Béthoux, N., Mauffret, A. & Pascal, G., 2001. A Ligurian (Western Mediterranean Sea) geophysical transect revisited, *Geophys. J. Int.,* **146,** 74–97.

Courboulex, F. *et al*., 2007. Seismic hazard on the French Riviera: new data, interpretations and simulations, *Geophys. J. Int.,* **170**(1), 387–400.

DBMI, 2004. DataBase Macrosismico Italiano, http://emidius.mi.ingv.it/DBMI04/.

Denza, F., 1887. Alcune notizie sul terremoto del 23 febbraio 1887. Torino.

Dercourt, J. *et al*., 1986. Geological evolution of the Tethyan belts from Atlantic to Pamirs since the Lias, *Tectonophysics,* **123,** 241–315.

Dessa, J.X. *et al*., 2011. The GROSMarin experiment: three dimensional crustal structure of the North Ligurian margin from refraction tomography and preliminary analysis of microseismic measurements, *Bulletin de la Société Géologique de France,* **182,** 305–321, doi:10.2113/gssgfbull.182.4.305.

Déverchère, J., Béthoux, N., Hello, Y., Louat, R. & Eva, C., 1991. Déploiement d'un réseau de sismographes sous-marins et terrestres en domaine Ligure (Méditerranée): campagne SISBALIG 1, *Comptes Rendus de l'Académie des Sciences de Paris,* **313,** 1023–1030.

Déverchère, J. *et al*., 2005. Active thrust faulting offshore Boumerdes, Algeria, and its relations to the 2003 M_w 6.9 earthquake, *Geophys. Res. Lett.,* **32,** L04311, doi:10.1029/2004GL021646.

Dewey, J., Helman, M., Turco, E., Hutton, D. & Knott, S., 1989. Kinematics of the western Mediterranean, in *Alpine Tectonics,* Geol. Soc. Lond. Spec. Pub. Vol. 45, pp. 265–283, eds Coward, M., Dietrich, D. & Parks, G.G., Geological Society, London.

Doglioni, C., Gueguen, E., Sàbat, F. & Fernandez, M., 1997. The western Mediterranean extensional basin and the alpine orogen, *Terra Nova,* **9,** 109–112.

Dubar, M., Innocent, C. & Sivan, O., 2008. Radiometric dating (U/Th) of the lower marine terrace (MIS 5.5) west of Nice (French Riviera): morphological and neotectonic quantitative implications, *Comptes Rendus Geoscience,* **340,** 723–731, doi:org/10.1016/j.crte.2008.07.012.

Edel, J.B., Dubois, D., Marchant, R., Hernandez, J. & Cosca, M., 2001. La rotation miocène inférieure du bloc corso-sarde; nouvelles contraintes paléomagnétiques sur la fin du mouvement, *Bulletin de la Société Géologique de France,* **172**(3), 275–283.

Efron, B., 1982. The jackknife, the bootstrap and other resampling plans, *CBMS-NSF Regional Conference Series in Applied Mathematics,* p. 92, Society for Industrial and Applied Mathematics, Philadelphia, PA.

Eva, C. & Rabinovich, A.B., 1997. The February 23, 1887 tsunami recorded on the Ligurian coast, western Mediterranean, *Geophys. Res. Lett.,* **24,** 2211–2214.

Eva, E. & Solarino, S., 1998. Variations of stress directions in the western Alpine arc, *Geophys. J. Int.,* **135,** 438–448.

Eva, E., Solarino, S. & Spallarossa, D., 2001. Seismicity and crustal structure beneath the western Ligurian Se derived from local earthquake tomography, *Tectonophysics,* **339,** 495–510.

Faccenna, C., Mattei, M., Funicello, R. & Jolivet, L., 1997. Styles of back-arc extension in the Central Mediterranean, *Terra Nova,* **9,** 126–30.

Fanucci, F. & Nicolich, R., 1984. Il Mar Ligure: nuove acquisizioni sulla natura, genesi ed evoluzione di un "Bacino marginale", *Mem. Soc. Geol. It.,* **27,** 97–110.

Federici, P.R. & Pappalardo, M., 2006. Evidence of marine isotope stage 5.5 highstand in Liguria (Italy) and its tectonic significance, *Quater. Int.,* **145,** 68–77.

Ferrari, G., 1991. The 1887 Ligurian earthquake: a detailed study from contemporary scientific observations, *Tectonophysics,* **193,** 131–139.

Ferry, M., Meghraoui, M., Delouis, B. & Giardini, D., 2005. Evidence for Holocene paleoseismicity along the Basel-Reinach active normal fault (Switzerland): a seismic source for the 1356 earthquake in the Upper Rhine graben, *Geophys. J. Int.,* **160,** 554–572.

Fines, M., 1887. Sur le Tremblement de terre du 23 février 1887, enregistré à l'observatoire de Perpignan, *Comptes Rendus de l'Académie des Sciences de Paris,* **104,** 606–608.

Fryer, G.J., Watts, P. & Pratson, L.F., 2004. Source of the great tsunami of 1 April 1946: a landslide in the Aleutian forearc, *Mar. Geol.,* **203,** 201–208.

Gasperini, P., Bernardini, F., Valensise, G. & Boschi, E., 1999. Defining seismogenic sources from earthquake felt report, *Bull. seism. Soc. Am.,* **89,** 94–110.

Gattacceca, J., Deino, A., Rizzo, R., Jones, D.S., Henry, B., Beaudoin, B. & Valeboin, F., 2007. Miocene rotation of Sardinia: new paleomagnetic and geochronological constraints and geodynamic implications, *Earth planet. Sci. Lett.,* **258,** 359–377.

Guidoboni, E., Ferrari, G., Mariotti, D., Comastri, A., Tarabusi, G. & Valensise, G., 2007. CFTI4MED, Catalogue of Strong Earthquakes in Italy (461 B.C.-1997) and Mediterranean Area (760 B.C.-1500). INGV-SGA, http://storing.ingv.it/cfti4med/.

Hassoun, V., Migeon, S., Cattaneo, A., Larroque, C. & Mercier de Lépinay, B., 2009. Imbricated scars on the Ligurian continental slope: evidence for multiple failure events in the 1887 earthquake epicentral area. International Conference on Sea Floor Mapping for Geohazard Assessment (session 4), Forio d'Ischia (Italy) may 11–13, *Rendiconti online della Societa Geologica Italiana,* **7,** 109–112.

Ilayaraja, K., Ioualalen, M., Chlieh, M., Krishnamurthy, R.R. & Ramanamurthy, M.V., 2008. Numerical modelling of the 26th December 2004 Indian Ocean tsunami at Andaman and Nicobar Islands, *J. Coast. Conserv,* doi:10.1007/s11852-008-0033-8.

Ioualalen, M., 2008. Séismes,tsunamis et leur calibration: cas de l'événement de Sumatra du 26 Décembre 2004, *La houille Blanche, La Revue Internationale de l'Eau.,* Société Hydrotechnique de France, doi:10.1051/lhb:2008002.

Ioualalen, M., Pelletier, B., Watts, P. & Regnier, M., 2006. Numerical modelling of the 26th November 1999 Vanuatu tsunami, *J. geophys. Res.,* **111,** C06030, doi:10.1029/2005JC003249.

Ioualalen, M., Asavanant, J., Kaewbanjak, N., Grilli, S.T., Kirby, J.T. & Watts, P., 2007. Modelling of the 26th December 2004 Indian Ocean

tsunami: case study of impact in Thailand, *J. geophys. Res.,* **112,** C07024, doi:10.1029/2006JC003850.

Ioualalen, M., 2009. Sensitivity tests on relations between the tsunami signal and seismic rupture characteristics; the 26 December 2004 Indian Ocean event case study, *Environ. Model. Softw.,* **24,** 1354–1362, doi:10.1016/j.envsoft.2007.07.007.

Ioualalen, M., Rentería, W., Ilayaraja, K., Chlieh, M. & Arreaga-Vargas, P., 2010a. Case study of impact of the 26th December 2004 Indian Ocean Tsunami on the coast of Sri Lanka, *Environ. Model. Softw.,* doi:10.1016/j.envsoft.2010.04.010.

Ioualalen, M., Arreaga-Vargas, P., Pophet, N., Chlieh, M., Ilayaraja, K., Ordoñez, J., Renteria, W. & Pazmiño, N., 2010b. Numerical modelling of the 26th December 2004 Indian Ocean tsunami for the South-Eastern coast of India, *Pure appl. Geophys.,* doi:10.1007/s00024-010-0053-9.

Ioualalen, M., Migeon, S. & Sardou, O., 2010c. Landslide tsunami vulnerability in the Ligurian Sea: case study of the 1979 October 16 Nice international airport submarine landslide and of identified geological mass failures, *Geophys. J. Int.,* **181,** 724–740, doi:10.1111/j.1365-246X.2010.04572.x.

Kennedy, A.B., Chen, Q., Kirby, J.T. & Dalrymple, R.A., 2000. Boussinesq modelling of wave transformation, breaking, and run-up. I: 1D, *J. Waterway, Port, Coastal, Ocean Eng.,* **126,** 39–47.

Lallemand, M., 1887. Observations du niveau de la Méditerranée, faites à Marseille le 23 février 1887, à l'instant du tremblement de terre, *Comptes Rendus hebdomadaires des séances de l'Académie des Sciences de Paris,* **104,** 764.

Lamarche, G., Lurton, X., Verdier, A.L. & Augustin, J.-M., 2011. Quantitative characterisation of seafloor substrate and bedforms using advanced processing of multibeam backscatter—application to Cook Strait, New Zealand, *Cont. Shelf Res.,* **31,** S93–S109, doi:10.1016/j.csr.2010.06.001.

Larroque, C., 2009. Aléa sismique dans une région intraplaque à sismicité modérée: la jonction Alpes – Bassin Ligure, Mémoire d'Habilitation à Diriger des Recherches, Université de Nice – Sophia Antipolis, 176 pp., http://tel.archives-ouvertes.fr/tel-00453377/fr/.

Larroque, C., Béthoux, N., Calais, E., Courboulex, F., Deschamps, A., Déverchère, J., Stéphan, J.F., Ritz, J.F. & Gilli, E., 2001. Active and recent deformation at the Southern Alps – Ligurian basin junction, *Neth. J. Geosci. – Geologie en Mijnbouw,* **80,** 255–272.

Larroque, C., Delouis, B., Godel, B. & Nocquet, J.M., 2009. Active deformation at the southwestern Alps–Ligurian basin junction (France-Italy boundary): evidence for recent change from compression to extension in the Argentera massif, *Tectonophysics,* **467,** 1–4, doi:10.1016/j.tecto.2008.12.013.

Larroque, C., Scotti, O. & Ioualalen, M., 2010. The 1887 earthquake and tsunami on the northern Ligurian margin (western Mediterranean), in *Proceedings of the European Seismological Commission, 32nd General Assembly,* Montpellier (France), September 6–10, abstract book, d0324_0553, 205.

Larroque, C., Delouis, B., Hippolyte, J.C., Deschamps, A., Lebourg, T., Courboulex, F. & Bellier O, 2011a. Joint multidisciplinary studies of the Saint Sauveur – Donareo fault (lower Var valley, French Riviera): a contribution to the seismic-hazard assessment in the urban area of Nice, *Bulletin de la Société Géologique de France,* **182,** 323–336, doi:10.2113/gssgfbull.182.4.323.

Larroque, C., Mercier de Lépinay, B. & Migeon, S., 2011b. Morphotectonic and fault-earthquake relationships along the northern Ligurian margin (Western Mediterranean) based on high resolution multibeam bathymetry and multichannel seismic-reflection profiles, *Mar. geophys. Res.,* **32,** 163–179, doi:10.1007/s11001-010-9108-7.

Larroque, C. & Sage, F., 2011. Active Deformation of the Northern Ligurian Margin (Western Mediterranean): faulting along inherited structures?, in *Proceedings of the 10th Alpine Workshop "CorseAlp 2011",* Saint Florent (Corsica), April 10–16, abstract volume, 47.

Le Pichon, X., 1982. Land-locked ocean basin and continental collision in eastern Mediterranean area as a case exemple, in *Mountain Building Processes,* pp. 201–213, ed. Hsu, K.J., Academic Press, San Diego, CA.

Levret, A. & Mohammadioun B., 1984. Determination of seismic reference motion for nuclear sites in France, *Eng. Geol.,* **20,** 25–38

Levret, A., Backe, J.C. & Cushing M., 1994. Atlas of macroseismic maps for French earthquakes with their principal characteristics, *Nat. Hazard,* **10,** 19–46.

Malinverno, A. & Ryan, W.B.F., 1986. Extension in the Tyrrhenian sea and shortening in the Apennines as a result of arc migration driven by sinking of the lithosphere, *Tectonics,* **5,** 227–245.

Mard Karisson, J., Skelton, A., Sanden, M., Ioualalen, M., Kaewbanjak, N., Pophet, N., Asavanant, J. & Von Matern, A., 2009. Reconstructions of the coastal impact of the 2004 Indian Ocean tsunami in the Khao Lak area, Thailand, *J. geophys. Res.,* **114,** C10023, doi:10.1029/2009JC005516.

Masson, F., Verdun, J., Bayer, R. & Debeglia, N., 1999. Une nouvelle carte gravimétrique des Alpes occidentales et ses conséquences structurales et tectoniques, *Comptes Rendus de l'Académie des Sciences de Paris,* **329,** 865–871.

McAdoo, B.G. & Watts, P., 2004. Tsunami hazard from submarine landslides on the Oregon continental slope, *Mar. Geol.,* **203,** 235–245.

McClusky, S., Reilinger, R., Mahmoud, S., Ben Sari, D. & Tealeb, A., 2003. GPS constraints on Africa (Nubia) and Arabia plate motions, *Geophys. J. Int.,* **155,** 126–138, doi:10.1046/j.1365-246X.2003.02023.

Mercier de Lépinay, B. *et al*., 2007. Active tectonic along the northern margin of the Ligurian sea: evidences from swath bathymetry and high-resolution seismic, in *Proceedings of the 38th CIESM Congress,* Istanbul, April 9–14 (Abstract volume).

Meunier, S., 1887. Observations relatives au tremblement de terre qui s'est fait sentir en Ligurie, le 23 février 1887, *Bulletin de la Société Géologique de France,* **15,** 459–463.

Meyer, B., Lacassin, R., Brulhet, J. & Mouroux, B., 1994. The Basel earthquake: which fault produced it ?, *Terra Nova,* **6,** 54–63.

Migeon, S., Cattaneo, A., Hassoun, V., Larroque, C. & Mercier de Lépinay, B., 2009. Submarine instabilities along the Ligurian Margin (NW Mediterranean): types, distribution and causes. International Conference on Sea Floor Mapping for Geohazard Assessment (session 4), Forio d'Ischia (Italy) may 11–13, 2009, *Rendiconti online della Societa Geologica Italiana,* **7,** 113–117.

Migeon, S., Cattaneo, A., Hassoun, V., Larroque, C., Corradi, N., Fanucci, F., Dano, A. & Mercier de Lepinay, B., 2011. Morphology, distribution and origin of recent submarine landslides of the Ligurian Margin (Northwestern Mediterranean): some insights into geohazard assessment, *Mar. geophys. Res.,* **32,** 163–179, doi:10.1007/s11001-011-9123-3.

Musson, R.M.W., Grunthal, G. & Stucchi, M., 2010. The comparison of macroseismic intensity scales, *J. Seismol.,* **14,** 413–428.

Naudin, C., 1887. Quelques observations et réflexions au sujet du tremblement de terre du 23 février à Antibes, *Comptes Rendus de l'Académie des Sciences de Paris,* **104,** 822–823.

Nocquet, J.M. & Calais, E., 2003. Crustal velocity field of Western Europe from permanent GPS array solutions, 1996–2001, *Geophys. J. Int.,* **154,** 72–88.

Nocquet, J.M. & Calais, E., 2004. Geodetic measurements of crustal deformation in the Western Mediterranean and Europe, *Pure appl. Geophys.,* **161,** 661–681.

Nocquet, J.M., Willis, P. & Garcia, S., 2006. Plate kinematics of Nubia-Somalia using a combined DORIS and GPS solution, *J. Geodyn.,* **80,** 591–607, doi:10.1007/s00190-006-0078-0.

Nodder, S.D., Lamarche, G., Proust, J.N. & Stirling, M.W., 2007. Characterizing earthquake recurrence parameters for offshore faults in the low strain, compressional Kapiti-Manawatu Fault System, New Zealand, *J. geophys. Res.,* **112,** B12102, doi:10.1029/2007JB005019.

Okada, Y., 1985. Surface deformation due to shear and tensile faults in a hallf-space, *Bull. seism. Soc. Am.,* **75,** 1135–1154.

Offret, A., 1887. Tremblement de terre du 23 février 1887. Heures de l'arrivée des secousses en dehors de l'épicentre, *Comptes Rendus de l'Académie des Sciences de Paris,* **104,** 1238–1242.

Pelinovsky, E., Kharif C., Riabov, I., & Francius, M., 2002. Modelling of tsunami propagation in the vincinity of the French coast of the Mediterranean, *Nat. Hazards,* **25,** 135–159.

Poirier, J.P., Perrier, F. & Le Mouël, J.L., 2008. On some electrical effects of the 1887 Ligurian earthquake, *Comptes Rendus Géosciences* **340,** 203–210, doi:10.1016/j.crte.2007.12.004.

Rebaï, S., Philip, H. & Taboada, A., 1992. Modern tectonic stress field in the Mediterranean region: evidence for variation in stress direction at different scales, *Geophys. J. Int.,* **110,** 106–140.

Réhault, J.P., Boillot, G. & Mauffret, A., 1984. The western Mediterranean basin geological evolution, *Mar. Geol.,* **55,** 447–477.

Reiter, L., 1990. *Earthquake Hazard Analysis: Issues and Insights,* p. 253, Columbia University Press, New York, NY.

Rollet, N., Déverchère, J., Beslier, M.O., Guennoc, P., Réhault, J.P., Sosson, M. & Truffert, C., 2002. Back arc extension, tectonic inheritance and volcanism in the Ligurian sea, Western Mediterranean, *Tectonics,* **21,** doi:10.1029/2001TC900027.

Sage, F. *et al*., 2011. Structure and evolution of a passive margin in a compressive environment: example of the south-western Alps-Ligurian basin junction during the Cenozoic, *Mar. Petrol. Geol.,* **28,** 1263–1282, doi:10.1016/j.marpetgeo.2011.03.012.

Schreiber, D., Lardeaux, J.M., Martelet, G., Courrioux, G. & Guillen, A., 2010. 3-D modelling of Alpine Mohos in Southwestern Alps, *Geophys. J. Int.,* **180,** 961–975.

Séranne, M., 1999. The Gulf of Lions continental margin (NW Mediterranean) revisited by IBS: an overview, in *On the Mediterranean Basins: Tertiary within Alpine Orogen,* Geol. Soc. Lond. Spec. Pub. Vol. 156, pp. 15–36, eds Durand, B., Jolivet, L., Horvath, F. & Séranne, M., Geological Society, London.

Serpelloni, E., Vannucci, G., Pondrelli, S., Argnani, A., Casula, G., Anzidei, M., Baldi, P. & Gasperini, P., 2007. Kinematics of the Western Africa-Eurasia plate boundary from focal mechanisms and GPS data, *Geophys. J. Int.,* **169,** 1180–1200, doi:10.1111/j.1365246X.2007.03367.x.

Sieberg, A., 1923. *Geologische, Physikalische und Angewandte Erdbebenkunde,* Gustav Fischer, Jena, 572 pp.

SISFRANCE, 2008. Histoire et caractéristiques des séismes ressentis en France, http://www.sisfrance.net/.

Speranza, F., Villa, I.M., Sagnotti, L., Florindo, F., Costentino, D., Cipollari, P. & Mattei, M., 2002. Age of the Corsica-Sardinia rotation and Liguro-Provençal basin spreading: new paleomagnetic and Ar/Ar evidence, *Tectonophysics,* **347,** 231–251.

Soloviev, S.L., 1990. Tsunamigenic zones in the Mediterranean Sea, *Nat. Hazard,* **3,** 183–202.

Stephan, E., 1887. Le tremblement de terre du 23 février 1887, à l'observatoire de Marseille, *Comptes Rendus de l'Académie des Sciences de Paris,* **104,** 556–557.

Taramelli, T. & Mercalli, G., 1888. Il terremoto ligure del 23 febbraio 1887, *Annali dell'Ufficio Centrale Meteorologico e Geodinamico Italiano, II,* **8**(4), 331–626.

Thouvenot, F., Paul, A., Fréchet, J., Béthoux, N., Jenatton, L. & Guiguet, R., 2007. Are there really superposed Mohos in the south-western Alps ? New seismic data from fan-profiling reflections, *Geophys. J. Int.,* **170,** 1180–1194, doi:10.1111/j.1365-246X.2007.03463.x.

Tinti, S., Vittori T. & Mulargia, F., 1987. On the macroseismic magnitudes of the largest Italian earthquakes, *Tectonophysics,* **138,** 159–178.

Tinti, S., Maramai, A. & Graziani, L., 2004. The new catalogue of Italian tsunami, *Nat. Hazard,* **33,** 439–465.

Triep, E.G., Abers, G.A., Lerner-Lam, A.L., Mishatkin, V., Zakharchenko, N. & Starovoit, O., 1995. Active thrust front of the Greater Caucasus: the April 19, 1991, Racha earthquake sequence and its tectonic implications, *J. geophys. Res.,* **100**(B3), 4011–4033.

Turino, C., Scafidi, D., Eva, E. & Solarino, S., 2009. Inference on active faults at the Southern Alps-Ligurian basin junction from accurate analysis of low energy seismicity, *Tectonophysics,* **475,** 470–479.

Vogt, J., 1992. Le «complexe» de la crise sismique nissarde de 1564, *Quaternaire,* **3,** 125–127.

Von Huene, R., Ranero, C.R. & Watts, P., 2004. Tsunamigenic slope failure along the Middle America Trench in two tectonic settings, *Mar. Geol.,* **203,** 303–317.

Wie, G. & Kirby, J.T., 1995. Time-dependent numerical code for extended Boussinesq equations, *J. Waterway, Port, Coastal, Ocean Eng.,* **121,** 251–261.

Wie, G., Kirby, J.T., Grilli, S.T. & Subramanya, R., 1995. A fully nonlinear Boussinesq model for free surface waves. Part 1: highly nonlinear unsteady waves, *J. Fluid Mech.,* **294,** 71–92.

Wells, D.L. & Coppersmith, K.J., 1994. New empirical relationships among magnitude, rupture length, rupture width, rupture area and surface displacement, *Bull. seism. Soc. Am.,* **84,** 974–1002.

Westphal, M., Orsini, J. & Vellutini, P., 1976. Le microcontinent corso-sarde, sa position initiale, données paléomagnétiques et raccords géologiques, *Tectonophysics,* **30,** 41–57.